Community composition and photophysiology of phytoplankton assemblages in coastal Oyashio waters of the western North Pacific during early spring

Kazuhiro Yoshida[1], Hisashi Endo[1,2,3], Evelyn Lawrenz[4], Tomonori Isada[5], Stanford B. Hooker[6], Ondřej Prášil[4], and Koji Suzuki[1,2]

[1]Graduate School of Environmental Science, Hokkaido University, North 10 West 5, Kita-Ku, Sapporo, Hokkaido 060-0810, Japan

[2]Faculty of Environmental Earth Science, Hokkaido University, North 10 West 5, Kita-Ku, Sapporo, Hokkaido 060-0810, Japan

[3]Bioinformatics Center, Institute for Chemical Research, Kyoto University, Gokasho, Uji, Kyoto 611-0011, Japan

[4]Laboratory of Photosynthesis, Institute of Microbiology, Czech Academy of Sciences, Opatovický mlýn, 37981 Třeboň, Czech Republic

[5]Akkeshi Marine Station, Field Science Center for Northern Biosphere, Hokkaido University, Aikkappu 1, Akkeshi-cho, Akkeshi-gun, Hokkaido 088-1113, Japan

[6]Goddard Space Flight Center, National Aeronautical and Space Administration, 8880 Greenbelt Rd, Greenbelt, MD 20771, USA

Correspondence to K. Yoshida (kyoshida711@ees.hokudai.ac.jp) and K. Suzuki (kojis@ees.hokudai.ac.jp)

Keywords: coastal Oyashio, spring diatom bloom, *P-E* curve, Diatom-specific *rbcL*, Chlorophyll *a* fluorescence

Abstract

Within the world ocean, the western subarctic Pacific is known as the region with the largest seasonal drawdown in the partial pressure of CO_2 due to biological activity, i.e., high spring primary production and particulate organic carbon flux. These distinctive features are mainly caused by intense spring diatom blooms in coastal Oyashio (COY) and Oyashio (OY) waters. Although phytoplankton assemblages in OY waters are rather well studied, little is known about COY waters. In this study, photophysiological properties and phytoplankton community composition in COY waters were investigated during the pre-bloom and bloom periods from March to April 2015. Next-generation sequencing targeting the 18S rRNA gene revealed that the diatom *Thalassiosira* generally dominated the phytoplankton community and showed distinct differences in the diatom communities in shelf and offshore waters of the COY. Additionally, the

relative contribution of *Thalassiosira* to the total diatom assemblages showed a positive correlation with maximum photosynthetic rates (P^{B}_{max}) occurring throughout this study. Chlorophyll *a* concentration and primary productivity were also positively correlated with sea surface temperature, suggesting that temperature was a critical factor for bloom development. Short-term on-deck incubation experiments were carried out to examine the role of temperature in determining planktonic photosynthetic processes. Our results showed an increase in P^{B}_{max} with rising temperature in assemblages from the shelf COY waters. Similarly, transcription levels of the diatom-specific *rbcL* gene, which encodes the large subunit of RuBisCO, also increased with rising temperature in the shelf assemblages. In contrast, temperature had little effect on the maximum photochemical quantum efficiency (F_v/F_m) of photosystem II. The results suggested that the transcription activity of the diatom-specific *rbcL* gene was upregulated by the increase in temperature, and that led to the higher P^{B}_{max} values and the spring diatom bloom in the shelf COY region.

1. Introduction

Photosynthetic marine phytoplankton are responsible for about half of the global primary production (Field et al., 1998; Behrenfeld et al., 2001) and are one of the principal drivers for the global carbon cycle (e.g. Sarmiento and Siegenthaler, 1992; Falkowski, 1994; Smetacek, 1999). The western subarctic Pacific has one of the highest transport efficiencies of particulate organic carbon (POC) in the water column (Honda et al., 2003; Kawakami et al. 2004; 2015) and the largest biological effect on seasonal changes in surface pCO_2 drawdown in the world ocean (Takahashi et al., 2002). These remarkable biogeochemical features are partly caused by large to vast spring diatom blooms observed in Oyashio (OY) and coastal Oyashio (COY) waters (Chiba et al., 2004; Hattori-Saito et al., 2010; Yoshie et al., 2010; Suzuki et al., 2011), which are biologically highly productive during spring (Isoda and Kishi, 2003; Isada et al., 2010). The OY is the westernmost current of the Western Subarctic Gyre (WSG) and is influenced by both the Eastern Kamchatka current and the Okhotsk Mode water (Yasuda, 2003; Oguma et al., 2008). The COY, on the other hand, is also derived from sea ice meltwater within the Sea of Okhotsk (Sugiura 1956; Ohtani 1971; Ogasawara 1990) flowing along the southeastern coast of Hokkaido in spring (Kono, 1997; Kono et al., 2004; Oguma et al., 2008; Kusaka et al., 2013). Consequently, COY waters can generally be distinguished from the OY by their lower salinity (< 33) and lower temperature (– 1.8 to 2 ºC) as the result of the sea ice meltwater in spring (Ohtani, 1971).

A number of studies have addressed the bloom dynamics in the OY region. For example, Suzuki et al. (2011) studied the community composition and bloom dynamics in OY waters and revealed that the annual spring bloom was often dominated by large, including chain-forming diatoms such as *Thalassiosira*, *Chaetoceros* and *Fragilariopsis* species. It was pointed out that development of steep density gradients in the water column (i.e., stratification) in spring can be associated with the initiation of the spring blooms in OY waters following the high nutrient supply into the surface mixed layer by winter deep mixing (Yoshimori et al., 1995; Kasai et al., 1997). Yoshie et al. (2003) noted that the deep mixing can significantly affect the amplitude of the spring OY bloom not only by the supply of nutrients but also by the dilution of predators, which drastically reduces grazing pressure (see Behrenfeld, 2010). Indeed, macrozooplankton grazing has a great impact on phytoplankton abundance, influencing the dynamics of the spring blooms in OY waters (Kasai et al., 1997; Saito et al., 2002; Kono and Sato, 2010). Saito et al. (2002) and Saito and Tsuda (2003) also proposed that light and silicate limitations could control the bloom dynamics in the OY region, particularly the initiation and termination of the spring diatom blooms. The spring diatom blooms in the OY waters can effectively foster the high productivity of higher trophic levels in this region (Taniguchi, 1999; Sakurai, 2007; Ikeda et al., 2008).

In contrast, fewer studies have been conducted in COY waters (Yoshimori et al., 1995; Kasai et al., 1997), even though the spring diatom blooms in COY waters have generally greater

91 magnitude than those in OY waters (Isada et al., 2010; Okamoto et al., 2010) and contributes
92 considerably to fisheries and aquaculture in this region (Nishimura et al., 2002; Isoda and Kishi,
93 2003). Like in OY waters, water column stratification may be highly relevant to the initiation of
94 the bloom in COY waters (Kasai et al., 1997). Yoshimori et al. (1995) noted that the blooms in
95 COY waters can exist for a longer time than those in OY waters due to continuous nutrient supply
96 with its weaker vertical stability. The phytoplankton bloom in COY waters would significantly
97 affect primary production in surrounding waters including the OY by physical processes such as
98 advection and eddy diffusion (Shinada et al., 1999; Okamoto et al., 2010). These pilot studies on
99 the spring blooms in COY waters investigated relationships among physical and biological
100 parameters for estimating the bloom dynamics, but no study has been conducted to investigate
101 the photophysiology and community composition of phytoplankton in COY waters. Low
102 temperatures observed in COY waters can decrease growth rates and the photosynthesis of
103 phytoplankton (Eppley, 1972; Raven and Geider et al., 1998). In addition, low temperatures in
104 COY waters could be far below the thermal optimum for the carbon fixing enzyme of the Calvin
105 cycle, Ribulose 1, 5- bisphosphate carboxylase/oxygenase (RuBisCO) (Descolas-Gros and de
106 Billy, 1987; Young et al., 2015). In spite of low temperatures, however, intense and extensive
107 diatom blooms are observed in COY waters every spring. Corresponding to the different origins
108 of COY and OY waters, it can be expected that the composition of diatoms may also be distinct

between these two water masses. Regarding zooplankton community, significant differences in community composition were reported at the species level between these water masses (Yamaguchi et al., 2003; Abe et al., 2014), however, information about possible differences in phytoplankton community composition are still missing.

From the aforementioned results, we hypothesized that (i) phytoplankton community composition in COY waters is distinctly different from offshore regions, and (ii) low temperatures in COY waters inhibit phytoplankton photosynthesis, specifically carbon fixation processes. In regards to the latter, we expect the subsequent warming of the water column during spring enhances photosynthetic activity. In this study, phytoplankton community composition in COY waters during spring was assessed with both phytoplankton pigment signatures and DNA-based next-generation sequencing (NGS) technology. Pigment analysis using the Suzuki et al. (2015) method of ultra-high performance liquid chromatography (UHPLC) allowed us to estimate the community composition of phytoplankton assemblages at the class level, whereas the relative contributions of each diatom genus to the total biomass of diatoms were quantified with the NGS method. In addition, the photophysiology of phytoplankton in COY waters during the pre-bloom and bloom periods were investigated using the following: a) active chlorophyll fluorescence techniques, e.g., pulse amplitude modulated (PAM) and fast repetition rate (FRR) fluorometry; b) the transcription activity of the diatom-specific *rbcL* gene, which encodes the large subunit of

127 RuBisCO; c) carbon-based photosynthesis-irradiance (*P-E*) curve experiments; and d) 77K
128 emission spectroscopy. The active chlorophyll fluorescence techniques enabled us to measure
129 photosynthetic activities (i.e., the maximum quantum yield of photochemistry) in photosystem II
130 (hereafter PSII). On the other hand, transcription levels of the diatom-specific *rbcL* gene
131 determined by reverse transcribed quantitative PCR can be used as an indicator for the activity of
132 the light independent reactions of photosynthesis because RuBisCO encoded by the *rbcL* gene is
133 the rate-determining enzyme of the process (John et al., 2007). Moreover, carbon-based *P-E*
134 curves provide powerful insights into photophysiological states such as photoacclimation and
135 nutrient stress (Sakshaug et al., 1997; MacIntyre et al., 2002) through the whole photosynthetic
136 processes from light absorption to carbon fixation. Emission spectroscopy also provided
137 semiquantitative information about the presence of major taxonomic groups and the physiological
138 status of phytoplankton. The combination of these techniques provides us with holistic
139 information on the photosynthetic processes of phytoplankton in COY waters. To elucidate the
140 photophysiological responses of phytoplankton to temperature, we also performed, for the first
141 time ever, temperature-controlled bottle incubation experiments in COY waters.
142
143 2. Materials and methods
144 2-1. Water sampling and optical observation
145 Seawater samples were collected from the western subarctic Pacific off the southeastern

146 Hokkaido (Japan) coast as part of the R/V *Hakuho Maru* KH15-1 expedition during 6–26 March
147 2015 and the TR/V *Misago Maru* field study (hereafter AK15 expedition) during 16–17 April
148 (Fig. 1). Prior to water sampling during the KH15-1 expedition, vertical profiles of
149 photosynthetically available radiation (PAR) spanning 400−700 nm, E_d(PAR) and spectral
150 downward irradiance, $E_d(\lambda)$, were obtained with the Compact-Optical Profiling System (C-OPS)
151 co-developed by Biospherical Instruments Inc. and NASA (Hooker et al., 2013). Vertical
152 attenuation coefficients of downward PAR, K_d (PAR) were determined as the slopes of a least-
153 squares regression of the natural-log transformed E_d(PAR) profiles using Processing of
154 Radiometric Observation of Seawater using Information Technologies (PROSIT) software
155 (Hooker, 2014). Based on the derived K_d (PAR) value, euphotic zone depth (Z_{eu}) was calculated
156 as the depth with 1% of the surface PAR remaining (Kirk, 2010). The incident PAR above the sea
157 surface (E_0) was measured on-deck continuously with an LI-190SB air quantum PAR sensor and
158 recorded by a LI-1400 data logger (LI-COR, Inc.) every 5−10 min. Surface (~5 m depth) seawater
159 samples were obtained using a CTD carousel multi-sampler system (CTD-CMS) with acid-
160 cleaned Niskin bottles. Upon collection, seawater was poured into a 9 L polycarbonate (PC)
161 carboy, four 300 mL PC bottles for the measurements of primary productivity, and two
162 polystyrene tubes for nutrient analyses. Concentrations of nutrients (nitrate + nitrite, ammonia,
163 phosphate, and silicate) were determined with a BRAN-LUEBEE autoanalyzer (QuAAtro).

Mixed layer depths (MLD) at all stations were calculated as the depth at which the potential density anomaly ($\Delta\sigma_\theta$) of the water column increased by 0.125 kg m^{-3} relative to the layer at 10 m (Monterey and Levitus, 1997).

2-2. Phytoplankton pigment composition

Seawater was dispensed into two 1 L PC bottles and these subsamples were filtered onto GF/F filters using a gentle vacuum (< 0.013 MPa). Filters were then blotted dry between filter papers, placed into cryovials, and immediately frozen in liquid nitrogen. Frozen filters were stored at –80 ºC until further analysis. Pigments were extracted with the *N*, *N*-dimethylformamide (DMF) sonication method of Suzuki et al. (2002). Pigment concentrations were then determined by high-performance liquid chromatography (HPLC) or UHPLC following Van Heukelem and Thomas (2001) with a few modifications and Suzuki et al. (2015), respectively. To estimate phytoplankton community composition at the class level, multiple linear regression analyses based on major diagnostic pigment signatures and chlorophyll *a* (Chl *a*) were performed following Suzuki et al. (1997) and Obayashi et al. (2001), wherein fucoxanthin (Fuco) and peridinin (Peri) are representative algal marker pigment for diatoms and dinoflagellates, respectively. Although Fuco can also be observed in other phytoplankton taxa, e.g., chrysophytes, haptophytes and some dinoflagellates, we assumed Fuco was solely derived from diatoms in this study. This assumption

can be justified with the results of Suzuki et al. (2011) who found a significant relationship between Fuco and diatom carbon during a spring bloom study in the study area. The following multiple linear regression of pigment markers was used:

$$[\text{Chl } a] = A[\text{Fuco}] + B[\text{Peri}] + C, \quad (1)$$

wherein [Chl *a*], [Fuco], and [Peri] are the concentrations of each pigment; *A* and *B* are partial regression coefficients for each concentration of the pigment markers; and *C* is a constant term of the multiple linear regression. The multiple linear regression analysis, and its validation with a *t*-test for each coefficient plus *F*-test, were performed with SigmaPlot software program ver. 11.0 (System Software). After this procedure, the contributions of each phytoplankton taxon to the total Chl *a* level were calculated by dividing a product of each concentration of pigment and its coefficient value by [Chl *a*] for each station.

2-3. Size-fractioned Chl *a* concentration

Seawater samples were filtered onto a 47 mm nylon mesh (20 µm pore size), a 47 mm Nuclepore membrane (10 or 2 µm pore size) and a 25 mm Whatman GF/F filter (nominal pore size 0.7 µm) using a gentle vacuum (<0.013 MPa). After filtration, filters were placed in cryovials, immediately flash frozen in liquid nitrogen, and stored at –80 ºC until further analysis. After thawing, the filters were transferred into glass cuvettes and soaked in 6 mL DMF at –20 ºC for at

200 least 24 h to extract phytoplankton pigments (Suzuki and Ishimaru, 1990). Chl *a* concentrations
201 were determined with a Turner Designs 10-AU fluorometer using the non-acidification method
202 of Welschmeyer (1994). The three size classes were defined as microphytoplankton (>20 μm),
203 nanophytoplankton (2–20 μm), and picophytoplankton (0.7–2 μm).
204
205 2-4. Ion Torrent next-generation sequencing (NGS)
206 Seawater samples for DNA analysis were collected sequentially on 25 mm polycarbonate
207 Isopore filters (Millipore, 2 μm pore size) with a gentle vacuum (< 0.013 MPa) and then stored at
208 - 80 ºC until further analysis. DNA samples were extracted using the method of Endo et al.
209 (2013). Extracted DNA samples were purified using a NucleoSpin® gDNA Clean-up (Macherey-
210 Nagel) following the manufacturer's protocols. The extracted DNA was sequenced with an Ion
211 Torrent Personal Genome Machine (PGM) targeting the diatom-specific 18S rRNA gene V4
212 region. NGS libraries of DNA were constructed for each sample obtained from all stations and
213 from the temperature-controlled incubation experiments. Gene fragments of the diatom-specific
214 18S rRNA V4 region sequences were amplified with the Takara Ex Taq Hot Start Version
215 (Takara) and diatom-specific fusion primer pairs with 12 barcodes:
216 Forward primer: 5'-GATGATGARAAYATTAACTCW-3'
217 Reverse primer: 5'- TAWGAACCTTTWACTTCWCC-3'

The forward primer included the A-adapter sequence (5'-CCATCTCATCCCTGCGTGTCTCCGAC-3'), the key sequence (5'-TCAG-3'), the barcode sequences set by the manufacturer (Thermo Fisher Scientific) and a barcode adapter sequence (5'-GAT-3') upstream of the forward primer. The reverse primer included the truncated Pi-adapter (trP1: 5'-CCTCTCTATGGGCAGTCGGTGAT-3') sequence upstream of the reverse primer. PCR mixtures consisted of 1× Ex Taq Buffer, 0.2 mM dNTP, 0.4 μM of the fusion primers, 0.625 unit of Taq polymerase, and 2 μL DNA template for a 25 μL total volume. PCR cycles within a thermal cycler were performed using the following conditions: 94 ºC for 60 s, 30 cycles under 98 ºC for 10 s, 56 ºC for 30 s, and 72 ºC for 60 s. After the final cycle, the temperature was held at 72 ºC for 10 min to complete the PCR reactions. PCR products were purified with an Agencourt AMPure XP Kit (Beckman Coulter) and 70 % ethanol following the manufacturer's protocols. The concentration of the purified amplicons was determined with an Agilent 2100 Bioanalyzer (Agilent Technologies) using an Agilent 1000 Assay Kit according to the manufacturer's protocol. Based on the results of the Bioanalyzer, the purified amplicons were diluted to a concentration of 13 pM. Once NGS libraries were constructed, emulsion PCR was conducted with an Ion One Touch 2 system and an Ion PGM Template OT2 400 kit (Thermo Fisher Scientific). The resultant emulsion PCR products were then enriched with Ion One Touch ES (Thermo Fisher Scientific) according to the manufacturer's protocols. The enriched templates

were loaded onto an Ion 318 v2 chip (Thermo Fisher Scientific) and amplicon libraries were sequenced with an Ion Torrent PGM system using the Ion PGM sequencing 400 kit v2 (Thermo Fisher Scientific) following the manufacturer's protocols.

To remove sequences with low quality and polyclonal sequences which did not match the A-adapter, quality filtering was initially performed with the Torrent Suite™ Software (Thermo Fisher Scientific). Additionally, inapplicable sequencing reads which unmatched the trP1 adapter sequence and the reverse primer sequence were removed with the FASTX-Toolkit (http://hannonlab.cshl.edu/fastx_toolkit/). After removal of forward and reverse primers, reads between 18 and 270 bp were extracted as 18S rRNA V4 regions. In addition, reads with a quality score of less than 23 were also excluded from the analysis. The obtained sequences were exported as FASTQ files and then converted to FASTA files with the mothur v. 1.25.0 (Schloss et al., 2009) software.

Using the FASTA files obtained for taxonomic classification based on the diatom-specific 18S rRNA V4 region, representative 10,000 reads were deposited to the SILVAngs web interface (https://www.arb-silva.de). The reads were classified with >93% classification similarity to SILVA SSU Ref dataset 123.1. Data which did not match diatoms were excluded from the classification results. For full details of the sequencing methods, see Endo et al. (2016).

2-5. Variable Chl *a* fluorescence by PAM and FRR fluorometry

Seawater was dispensed in a 30 mL amber bottle and stored in the dark at ambient temperature for 30 min for dark acclimation to ensure fully open PSII reaction centers. After acclimation, samples were transferred to a quartz cuvette (15 mm pathlength) in a dark environment and placed inside a pulse amplitude modulation (PAM) fluorometer (Walz, Germany) and a fast repetition rate (FRR) fluorometer (Chelsea Technologies Group, West Mosley, UK) to determine the maximum quantum yield of photochemistry in PSII defined as F_v/F_{mPAM} and F_v/F_{mFRRf} for measurements made with the PAM and FRR fluorometers, respectively. In addition to F_v/F_{mFRRf}, the FRRf also provided measurements of the effective absorption cross sections of PSII, σ_{PSII}, and the concentration of functional PSII reaction centers, [RCII]. PAM and FRR fluorometry measurements were conducted on multiple subsamples from each sample (i.e., pseudo-replication) following Liu et al. (2009) for PAM fluorometry, and Kolber et al. (1998) and Oxborough et al. (2012) for FRRf fluorometry.

2-6. Light absorption coefficient of phytoplankton

Seawater was filtered onto Whatman GF/F filters using a gentle vacuum (< 0.013 MPa). After filtration, filters were carefully wrapped in aluminum foil to avoid any creases and then stored at -80 ºC until further analysis. Following Kishino et al. (1985), the optical density of particles and

detritus on the filters (OD_{fp} and OD_{fd}, respectively) was measured with a multipurpose scanning spectrophotometer (MPS-2450, Shimadzu) equipped with an end-on type photomultiplier tube in 1 nm steps from 350 to 800 nm before and after soaking filters in methanol for 15 min to remove phytoplankton pigments. Measurements before methanol extraction corresponded to the total absorption, those after methanol extraction to OD_{fd} and the difference between the two to OD_{fp}. All spectra were scatter corrected by subtracting the average value from 730 nm to 750 nm across the visible range (Babin and Stramski, 2002). Both OD_{fp} and OD_{fd} were converted to absorption coefficients, $a_p(\lambda)$ and $a_d(\lambda)$, respectively, using an appropriate path length amplification factor (Cleveland and Weidemann, 1993). The resultant $a_p(\lambda)$ values were then averaged from 400-700 nm and weighted to the spectral irradiance of the incubator lamp, $E_{PARinc}(\lambda)$ used for photosynthesis versus irradiance measurements to give mean absorption coefficients of phytoplankton ($\bar{a}_{ph}$) and mean Chl *a*-specific absorption coefficient of phytoplankton, $\bar{a}^*_{ph}(\lambda)$ following Isada et al. (2013).

2-7. Photosynthesis vs. Irradiance (*P*-*E*) curves and photosynthetic parameters

For each curve, seawater samples were dispensed into twelve 275 mL polystyrene bottles and inoculated with ca. 0.1 mg of $NaH^{13}CO_3$ (99 atom% ^{13}C purity, Cambridge Isotope Laboratories, Inc.). Two bottles at time zero remained without any isotope. Samples were then incubated in a

290 temperature-controlled incubator under 10 different light intensities between 1.44 and 1800 µmol
291 photons m^{-2} s^{-1} for 2 h under both, ambient or an altered temperature (see details below under
292 point 2-9). After incubation, samples were filtered onto pre-combusted 25 mm GF/F glass fiber
293 filters (Whatman), which were stored at -80 ºC until further analysis. Photosynthetic rates were
294 calculated from ^{13}C uptake rates measured with an on-line element analyzer (FlashEA1112,
295 Thermo Finnigan)/isotope ratio mass spectrometer (Delta-V, Thermo Finnigan) (EA/IRMS)
296 following Hama et al. (1983), normalized to Chl *a* and plotted versus irradiance. The resultant
297 P^B-E curves were fitted to the model of Platt et al. (1980):

298 $$P^B = P_s^B\left[1 - \exp\left(-\alpha^B \cdot E_{\text{PAR inc}}/P_s^B\right)\right] \cdot \exp\left(-\beta^B \cdot E_{\text{PAR inc}}/P_s^B\right), \text{ and}$$

299 $$P^B_{\max} = P_s^B \cdot [\alpha^B/(\alpha^B + \beta^B)] \cdot [\beta^B/(\alpha^B + \beta^B)]^{(\beta^B/\alpha^B)} \quad (2)$$

300 where, the superscript B denotes the biomass parameter used for normalization (here Chl *a*): P^B_{max}
301 [mg C mg Chl a^{-1} h^{-1}] is the maximum photosynthetic rate; α^B [(mg C mg Chl a^{-1} h^{-1}) (µmol
302 photons m^{-2} s^{-1})$^{-1}$] is the initial slope of the curve, or light utilization efficiency; $E_{PAR\ inc}$ [µmol
303 photons m^{-2} s^{-1}] is the PAR at each bottle in the incubator; β^B [(mg C mg Chl a^{-1} h^{-1}) (µmol
304 photons m^{-2} s^{-1})$^{-1}$] is the photoinhibition index; and P^B_s the maximum photosynthetic rate in the
305 absence of photoinhibition. The light saturation index, E_k [µmol photons m^{-2} s^{-1}] was calculated
306 as $E_k = P^B_{max}/\alpha^B$ and the maximum quantum yield for carbon fixation, Φ_{Cmax} [mol C mol photons^{-}
307 ^{1}] was also calculated as:

$$\Phi_{Cmax} = 0.0231\alpha^{B}/\bar{a}^{*}_{ph}, \quad (3)$$

with further details provided by Isada et al. (2013).

2-8. Primary productivity

Seawater was dispensed into four acid-cleaned 300 mL PC bottles, inoculated with ~0.1 mg of $NaH^{13}CO_3$ and incubated for 24 h in an on-deck incubator at ambient temperature, either at ambient irradiance (3 replicate samples) or in darkness (1 sample). After incubation, samples were filtered onto pre-combusted 25 mm GF/F glass fiber filters (Whatman) and stored at -80 ºC until further analysis as described above. Primary productivity, *PP* in the units of mg C m^{-3} day^{-1} for each sample was then calculated following Hama et al. (1983).

2-9. Temperature-controlled incubation experiments

To assess the effects of temperature on phytoplankton assemblages in COY waters, on deck temperature-controlled bottle incubation experiments were conducted using surface seawater collected from ca. 5 m depth, and dispensed into three 9 L PC carboys at stations Bio-6, Bio-7, Bio-10, and Bio-13 (Fig. 1). One of the three carboys was used for time zero samples, the remaining two were used to test for the effect of temperature, with ambient temperature being the control and +7 ºC being the high temperature treatment. To avoid any interference from possible

326 light effects, bottles were covered with black foil during the entire 24 h incubation. After
327 incubation subsamples were collected to determine diatom community composition by NGS
328 (Section 2-4) and to measure photosynthetic physiology by variable fluorescence and *P-E*
329 experiments (Sections 2-5 and 2-7) combined with analyses of the transcription level of the
330 diatom-specific *rbcL* gene by qRT-PCR(see following).
331
332 2-10. Transcription level of diatom-specific *rbcL* with qRT-PCR method
333 Sampling and extraction of DNA were performed as described above (Section 2-4). Seawater
334 for RNA samples was filtered onto 25 mm polycarbonate Isopore filters (Millipore, 2 μm pore
335 size) with a gentle vacuum (< 0.013 MPa). Filters for RNA analysis were placed in cryotubes
336 containing 0.2 g of pre-combusted 0.1 mm glass beads and 600 μL RLT buffer (Qiagen), to which
337 10 μL β-mercaptoethanol (Sigma-Aldrich) were added. After filtration, RNA samples were
338 immediately frozen in liquid nitrogen and stored at –80 °C until further analysis. RNA retained
339 on the filters were extracted following Endo et al. (2015). The extracted RNA was then reverse
340 transcribed into cDNA with the PrimeScriptTM RT Master Mix (RR036, Takara) according to
341 the manufacturer's specifications. Copy numbers of the diatom-specific *rbcL* gene in extracted
342 DNA and transcribed cDNA samples were quantified by quantitative PCR (qPCR) with standards
343 of the diatom-specific *rbcL* gene, which were produced from the diatom *Thalassiosira weissflogii*

344 (CCMP1336) in accordance with Endo et al. (2015).

345

346 2-11. Low temperature (77K) emission spectra

347 The emission spectra at 77K were measured on board using a custom-built portable emission
348 spectrometer (Prášil et al., 2009) and measuring procedures described in Hill et al. (2012) with
349 the following exceptions: the volume of seawater filtered on the 25 mm Whatman GF/F filters
350 was 1.2 L. For each sample, six emission spectra were collected, using LEDs with different
351 excitation wavelengths (390, 455, 470, 505, 530 and 590 nm). From each spectrum, a blank
352 spectrum (measured using filter soaked in distilled water) was subtracted.

353

354 2-12. Statistical analyses

355 Statistical analyses were conducted using the SigmaPlot software program ver. 11.0 (SystStat
356 Software, Inc.) except for the cluster analysis evaluating diatom community composition, which
357 was carried out in the statistical software R (http://www.r-project.org). Spearman's correlation
358 analysis was used to assess relationships between variables. Multiple linear regression analysis
359 was conducted to determine the contributions of each diatom group to total Chl *a*. Cluster analysis
360 was performed to investigate differences in community composition of diatoms using Bray-Curtis
361 dissimilarity and an average clustering method. Statistically significant differences between

362 clusters were assessed with a multivariate analysis of variance (MANOVA) test and the Wilks'
363 lambda discriminant analysis.
364
365 3. Results
366 3-1. Hydrographic conditions
367 Sea surface temperatures (SST) observed during the KH15-1 expedition were generally low
368 ranging from 0.0−1.6°C whereas higher SST between 2.4−3.8 ºC were observed during the AK15
369 cruise (Table 1). Values of sea surface salinity (SSS) were lower than 33 throughout both
370 expeditions with the lowest SSS value of 32.1 being observed at Station AK15-1 (Table 1).
371 Nutrients in surface waters were generally abundant during the KH15-1 expedition. The deepest
372 mixed layer depth (MLD) of 28.6 m was found at Station Bio-10 whereas the shallowest MLD of
373 15.8 m was found at Station Bio-6 (Table 1). During the KH15-1 expedition, the depth (z) of the
374 euphotic zone (Z_{eu}) was generally shallower than the MLD with Station Bio-6 being an exception
375 (Table 1).
376 Stations on the shelf ($z \leq 100$ m) were classified as shelf COY, whereas those in rather oceanic
377 regions ($z > 100$ m) were defined as offshore COY (Fig. 1 and Table 1). Warm water masses with
378 a relatively high temperature of ~4 ºC intruded into offshore COY waters from the western part
379 of the coast between the isopycnal surfaces (σ_θ = 26.7–26.8; Appendix A). Thus, we refer to these

stations as “Tokachi” to distinguish them from the other offshore and shelf sites.

3-2. Phytoplankton pigments

Concentrations of Chl *a* were generally <1 mg m^{-3} except at bloom stations Station Bio-14, AK15-1 and AK15-2 (hereafter bloom stations) (Fig. 2a). Chl *a* concentrations were positively correlated with SST, but negatively with SSS (Table 2). Fuco, Peri, and diadinoxanthin (DD) were the predominant carotenoids (Appendix B) and were used in the following multiple regression to derive total Chl *a* according to:

$$[\text{Chl } a] = 2.00\,[\text{Fuco}] + 1.78\,[\text{Peri}] + 0.107, \quad (4)$$

wherein $n = 21$, $r^2 = 0.994$, *t*-value for Fuco = 56.0 ($p < 0.001$), *t*-value for Peri = 2.85 ($p < 0.05$), *t*-value for the constant = 2.12 ($p < 0.05$), and $F = 367$ ($p < 0.001$). Diatoms were predominant at all sampling stations contributing between 54–96% of total Chl *a* and > 90% at the bloom stations (Fig. 3a).

3-3. Size-fractioned chlorophyll *a* concentration

Nanophytoplankton dominated the phytoplankton community during the KH15-1 expedition with the exception of the bloom stations and Station Bio-7, where microphytoplankton (>20 μm) dominated the phytoplankton assemblages. The lowest contribution (8.36 % of total Chl *a*) of

398 microphytoplankton was found at the farthest offshore Station Bio-10 (Fig. 3b).

399

400 3-4. Diatom community composition

401 The genera *Thalassiosira*, *Minidiscus*, *Skeletonema*, *Fragilariopsis*, and *Pseudo-nitzschia*
402 dominated the diatom assemblages (Fig. 4) with minor contributions of diatoms belonging to the
403 subdivision of Coscinodiscophytina. The genus *Thalassiosira* contributed >40% to the total Chl
404 *a* at the bloom stations (Bio-14, AK15-1 and AK15-2) and stations Bio-6 and Bio-7 (Fig. 4). Thus,
405 the composition of the diatom community at these shelf COY stations was significantly different
406 from that at other stations ($p < 0.01$, One-way MANOVA, Wilk's lambda; Fig. 5). At the offshore
407 COY and Tokachi stations, diatom communities were characterized by the dominance of
408 *Thalassiosira*, *Minidiscus* and/or *Fragilariopsis*.

409

410 3-5. Variable chlorophyll *a* fluorescence

411 $F_v/F_{m\ PAM}$ values determined with the PAM fluorometer varied between 0.17 – 0.55 (Fig. 2b),
412 giving an average of 0.35 ± 0.11 across all sites. The highest and lowest $F_v/F_{m\ PAM}$ values were
413 observed at Station AK15-1 and Bio-10, respectively. Also, $F_v/F_{m\ PAM}$ was significantly correlated
414 with Chl *a*, P^B_{max}, Φ_{Cmax}, and *PP*, (p <0.01, <0.01 <0.05, and <0.001, respectively; Spearman-
415 Rank correlation, Table 3). During the KH15-1 expedition, F_v/F_m measured by FRR fluorometry

($F_v/F_{m\ FRRf}$) (Appendix C) showed a similar spatiotemporal variation as $F_v/F_{m\ PAM}$ (ρ = 0.483, n = 20, p <0.05, Spearman-Rank correlation), although a large difference between $F_v/F_{m\ FRRf}$ and $F_v/F_{m\ PAM}$ was observed at Station Bio-1. Values of the functional absorption cross-section for PSII (σ_{PSII}) varied between 2.43 and 3.78 nm^2 $PSII^{-1}$. The lowest and highest values were observed at Stations Bio-14 and Bio-2, respectively, which deviated from values at the other stations. A much larger variability, however, was observed in the concentration of functional PS II centers [RCII], which varied between 0.49 $\times$ 10^{-9} and 5.57 $\times$ 10^{-9} mol m^{-3} at Station Bio-1 and Bio-14, respectively (Appendix C). The latter was also the site with the highest Chl *a* concentration.

3-6. Light absorption coefficient of phytoplankton

The Chl *a*-normalized light absorption coefficient for phytoplankton ($\bar{a}^*_{ph}$) at the bloom stations as well as at Station Bio-6 were relatively low compared to the other sites of this study (Fig. 2c). In particular, values of $\bar{a}^*_{ph}$ obtained during the AK15 cruise were one order of magnitude smaller than those during the KH15-1 expedition.

3-7. Low temperature (77K) emission spectra

We have observed significant variability among the 77K emission spectra collected at each station. The variability can be linked to species composition and the physiological state of

phytoplankton. An example of emission spectra in the 660 – 700 nm region is given in Appendix D, panels A and B. The phytoplankton emission in this spectral region is composed of several overlapping bands: the major band peaks at 685 nm and originates from PSII reaction centers, the band at 695 nm originates from active PSII containing CP47 (Suggett et al., 2009, D'Haene et al., 2015) and in some cases less intense bands at 675 and 680 nm were observed. In eukaryotic phytoplankton, the 680 nm band originates from loosely coupled antenna pigments with less efficient energy transfer to the PSII reaction center. The 675 nm band (Appendix D, panel B) is specific for emission from Peri containing peripheral peridinin-chlorophyll *a*-protein (PCP) antenna proteins in dinoflagellates and is excited only by the 500−600 nm wavelengths absorbed by PCP (Hill et al., 2012). Using simple analysis of the emission spectra based on the measured emission intensities at given wavelength, we have observed correlation ($r^2 = 0.598$) between the relative content of Peri (determined by UHPLC) and the increase of emission at 675 nm (Appendix D, panel C) or between the functional cross-section of PSII measured by FRR fluorometry and the intensity of the emission in the 675 – 680 nm region ($r^2 = 0.732$, see Appendix D, panel D). The increased emission band around 695 nm, indicating phytoplankton with active PSII (Suggett et al., 2009), was observed only at station Bio-14 (Appendix D, panel B).

3-8. *P-E* curves and their photosynthetic parameters

452 Values of α^B varied between 0.00949 – 0.0383 (mg C mg Chl a^{-1} h^{-1}) (µmol photons m^{-2} s^{-1})$^{-1}$

453 (Fig. 2d), and the β^B values ranged between 0.000628 – 0.00912 (mg C mg Chl a^{-1} h^{-1}) (µmol

454 photons m^{-2} s^{-1})$^{-1}$ (Fig. 2e). P^B_{max} values, however, were relatively constant and ranged between

455 1 – 2 mg C mg Chl a^{-1} h^{-1} except at the bloom stations (Fig. 2f). The E_k values varied from 83.2

456 to 235.0 µmol photons m^{-2} s^{-1} giving an average value with standard deviation of 131.8 ± 53.2

457 µmol photons m^{-2} s^{-1} (Fig. 2g). Values of Φ_{Cmax} were rather constant (0.0068 – 0.0275) except at

458 the bloom stations (Fig. 2h). The P^B_{max} and E_k showed negative correlations with respect to SSS

459 (Table 2).

460

461 3-9. Primary productivity

462 Primary productivity (*PP*) at all sampling stations ranged between 3.56 – 255.40 mg C m^{-3} d^{-1}

463 (Fig. 2i) being highest at the bloom stations. Lowest *PP* was observed at Station Bio-1, which

464 also had the lowest SST values (Fig. 2i, Table 1). Also note that *PP* was significantly correlated

465 with SST and Chl *a* (p<0.05 and <0.001, respectively, Spearman-Rank correlation, Tables 2, 3).

466

467 3-10. On-deck temperature-controlled bottle incubation experiments

468 Phytoplankton pigment signatures revealed that algal community composition calculated from

469 Eq. 4 changed relatively little (< 5%) during our incubations, except at Station Bio-6 where the

contribution of dinoflagellates increased from 39.7% to 47.7 % in the 7 °C treatment (Fig. 6). Similarly, little changes in the composition of diatoms occurred throughout all experiments except at Station Bio-13 (Tokachi waters) where growth of *Minidiscus* was stimulated in the 7 °C treatment (Fig. 7).

At the end of the incubation, the *P-E* curve parameters varied differently between incubations at different stations (Fig. 8). Values of α^{B} increased by ca. three-fold in the 7 °C treatment during the Bio-7 experiment, while changes at the other sites were much less pronounced (Fig. 8a). The P^{B}_{max} values increased in both treatments at most sites. The exception was Station Bio-10, where P^{B}_{max} showed a slight decrease in both the control and 7 °C treatment (Fig. 8c). Changes in E_k were variable increasing after incubation at 7 °C during experiments at stations Bio-6 and Bio10, but decreasing at Station Bio-7 (Fig. 8d). Φ_{Cmax} was highest in the +7 ºC treatment at Stations Bio-7 and Bio-13 (Fig. 8f). At the shelf COY (Bio-6 and Bio-7) and Tokachi (Bio-13) stations where the water was <100 m deep, values of the diatom-specific *rbcL* gene expression for the +7 ºC treatments were higher than those of the controls (Fig. 8g). Values of $\bar{a}^{*}_{ph}$ and F_v/F_{mPAM} varied little among treatments at all stations (Fig. 8e and h).

4. Discussion

4-1. Hydrography

488 Cold, low-salinity waters extended completely across our sampling sites throughout the
489 observation period i.e., early spring (Table 1). Following the water mass definitions in this study
490 area proposed by Ohtani (1971), OY waters were not detected. The results were similar to
491 observations of Kasai et al. (1997) who demonstrated that COY waters extended from the coast
492 off Hokkaido to the offshore station at 42º 40´ N, 144º 55´ E in March 1990, 1991, and 1992.
493
494 4-2. Abundance and community composition of spring phytoplankton in the COY
495 The temporal variation in Chl *a* concentration suggests that the sampling period covered both,
496 the pre-bloom and bloom phase (Fig. 2a), with the former being characterized by low Chl *a*
497 concentrations (<1 mg m^{-3}). The subsequent increase in Chl *a* concentration during the AK15
498 expedition represented the spring bloom at the shelf COY stations (Fig. 2a), which matches the
499 observations of Kasai et al. (1997) who also reported peaks in Chl *a* in COY waters in April.
500 Kasai et al. (1997) also proposed that shoaling of the MLD due to water-column stratification
501 may be an important factor for bloom initiation. In this study, however, there was no significant
502 relationship between any of the photosynthetic parameters (including Chl *a*) and MLD (Table 2).
503 The substantial increases in Chl *a* and Fuco at the bloom stations indicated that the blooms on the
504 COY shelf were dominated by diatoms (Fig. 3a and Appendix B). The large increase in the
505 relative contribution of microphytoplankton to the total phytoplankton also supports this notion

506 (Fig. 3b). Interestingly, our DNA sequencing analysis showed that the composition of the diatom
507 assemblages in most of the shelf COY stations differed from those of other water masses (Figs. 4
508 and 5). Because the shelf COY stations were located in relatively shallow waters, resuspension
509 of benthic diatoms from shelf sediments might affect either or both community composition and
510 bloom formation (e.g. McQuoid and Godhe, 2004), although no information on the composition
511 of the benthic algal community is available for our study area. The discrimination between the
512 shelf COY and other waters masses was based mainly on the presence and dominance of
513 *Thalassiosira* (Fig. 4). Shinada et al. (1999) observed *Thalassiosira* blooms in Funka Bay when
514 COY waters intruded into the bay in early spring. In this study, the genus *Thalassiosira* was the
515 bloom-forming species in the shelf COY waters indicated by the contribution of *Thalassiosira*
516 becoming high at the bloom stations (Fig. 4). The genera *Fragilariopsis* and *Minidiscus* were
517 relatively abundant in offshore COY and Tokachi waters (Fig. 4). Suzuki et al. (2011) reported
518 that the genus *Fragilariopsis* was abundant in OY waters. The substantial abundance of
519 *Minidiscus*, however, has not been reported in both COY and OY waters likely because the genus
520 *Minidiscus* can be overlooked with conventional light microscopy due to its small size, i.e.,
521 nanophytoplankton (Hasle and Syvertsen, 1996). Although blooms of the genus *Chaetoceros* are
522 commonly and annually observed during the bloom period (Mochizuki et al., 2002; Hattori-Saito
523 et al, 2010; Suzuki et al., 2011), the contributions of *Chaetoceros* to the diatom assemblages (as

524 determined with the next-generation sequencing method) were generally low and negligible
525 (<4%) (Fig. 4). Hattori-Saito et al. (2010) also observed the predominance of *Thalassiosira* at the
526 pre-bloom station at COY and OY regions, whereas *Cheatoceros* outcompeted other taxa at the
527 OY bloom station. Both pigment analysis (presence of peridinin, Appendix B) and 77K emission
528 spectroscopy (Appendix D, panel C) indicated increased presence of dinoflagellates at near-coast
529 stations Bio-6, 7 and 4.
530
531 4-3. Photosynthetic physiology of spring phytoplankton in the COY
532 At the bloom stations with high Chl *a* concentrations, we also observed high P^{B}_{max}, Φ_{Cmax}, and
533 *PP* values (Fig. 2a, f, h, and i), suggesting that the photophysiological states of phytoplankton had
534 improved from the pre-bloom period. In addition, P^{B}_{max} showed a significant correlation with
535 other photosynthetic parameters, i.e. F_v/F_{mPAM}, $\Phi_{Cmax,}$ and *PP* (Table 3). In turn, it should be noted
536 that the F_v/F_{mPAM} values correlated with *PP* and Chl *a* concentration as well (Table 3).
537 Consequently, light reaction processes in PSII are important for the underlying mechanisms such
538 as coupling of antenna pigments to PSII reaction centers (discussed below) to control *PP* and
539 phytoplankton biomass during the observation period. Indeed, the increase in [RCII] (i.e., the
540 concentration of PSII reaction centers) at Station Bio-14 indicated the significance of light
541 reaction processes in the bloom development (Appendix C). We also observed, for the first time,

correlations between the effective absorption cross-section of PSII (σ_{PSII}) and the relative intensity of the emission band at 680 nm that forms a low-wavelength shoulder of the main emission band assigned to PSII (see Appendix D, panels A and D). We assign this band to emission from antenna chlorophylls that are not tightly coupled to PSII reaction centers. We note that phytoplankton with high σ_{PSII} also shows a higher proportion of loosely coupled antenna pigments. Interestingly, at the high-chlorophyll station Bio-14 we detected both, low values of σ_{PSII}, a low proportion of uncoupled antenna and a significant increase in active PSII (see emission at 695nm, Appendix D, panels A and B). This enhanced coupling of antenna pigments at Station Bio-14 could lead the high F_v/F_m, P^B_{max} and *PP* values (Fig. 2b, f, and i), which might be associated with bloom development in COY waters. Interestingly, the SSS showed significant negative correlations with the photosynthetic parameters including P^B_{max} values and Chl *a* concentration (Table 2), which implies the surface phytoplankton assemblages in low saline shelf COY waters had relatively higher carbon fixation rates. Co-variations of the P^B_{max} and α^B values were not found in this study (Table 3), indicating E_k-dependent variability (Behrenfeld et al., 2004) in photosynthesis. According to Behrenfeld et al. (2004), the physiological mechanisms responsible for E_k-dependent variability generally involve acclimation strategies aimed at maximizing growth under variable light conditions. On the other hand, in the OY region, E_k-independent variability, which is the result of co-variation in P^B_{max} and α^B, was observed from March to May by Isada et al.

560 (2009) and in the post-bloom phase by Yoshie et al. (2010). Additionally, Yoshie et al. (2010)
561 pointed out that water temperature and ammonium levels significantly affected the E_k-
562 independent variability. In this study, water temperatures of COY remained relatively low (< 4°C;
563 Table 1) and ammonia did not influence any photosynthetic parameters (Table 2). The SST values,
564 however, showed significant positive correlations with Chl *a* and *PP*, suggesting that temperature
565 was a significant driver for biomass and primary production. The contribution of
566 microphytoplankton to total Chl *a* correlated positively with the photosynthetic parameters
567 including Chl *a*, F_v/F_{mPAM}, P^B_{max}, and *PP* (Table 2), indicating that microphytoplankton
568 contributed considerably to bloom formation in this area. The contributions of diatoms to Chl *a*
569 concentrations, however, did not show any significant correlation with these photosynthetic
570 parameters (Table 2). The results imply that some specific diatoms had different photosynthetic
571 strategies and formed the bloom in April. In fact, the contributions of *Thalassiosira* to the total
572 diatoms showed a positive relationship with P^B_{max} among the diatom groups (Table 2), which
573 suggests the genus *Thalassiosira* bloomed in COY waters.
574
575 4-3. Physiological response of phytoplankton to temperature in COY waters
576 In the temperature-controlled experiments, the phytoplankton assemblages showed different
577 responses among stations. Changes in the P^B_{max} values with the increase in temperature were

578 prominent for the phytoplankton assemblages in the shelf COY (Stations Bio-6 and -7) and the
579 Tokachi (Station Bio-13) waters, whereas no increase in P^{B}_{max} was observed for those in the
580 offshore COY at Station Bio-10 (Fig. 8c). Similarly, the diatom-specific *rbcL* cDNA copies
581 normalized by their DNA copies for the shelf COY and Tokachi assemblages also notably
582 increased after the temperature change (Fig. 8g), suggesting that the transcriptional levels of the
583 diatom-specific *rbcL* gene could be upregulated by the increase in temperature at these stations.
584 Interestingly, the offshore COY assemblages showed little change in the transcription level of
585 diatom-specific *rbcL* as well as P^{B}max (Fig. 8c and g). These concomitant increases indicate that
586 the enhancement of the P^{B}_{max} for the shelf COY and Tokachi assemblages could be caused by the
587 increases in the transcription level of the large subunit of RuBisCO with temperature. This
588 hypothesis is supported by the fact that P^{B}_{max} values are controlled by the activity of RuBisCO
589 (Li et al., 1984; Descolas-Gros and De Billy, 1987; Raven and Geider, 1998). In general, the
590 optimal temperature of RuBisCO (40 – 50 ºC) (Descolas-Gros and de Billy, 1987; Young et al.,
591 2015) was far above the *in situ* SST (0–4°C) observed in this study, and, thus, its activity would
592 increase exponentially with temperature up to a certain point (Descolas-Gros and de Billy, 1987;
593 Crafts-Brandner and Savucci, 2000). The temperature increase, therefore, enhanced both the
594 expression of the *rbcL* gene and the catalytic efficiency of RuBisCO, which eventually led to high
595 carbon fixation rates. The genus *Thalassiosira* became the bloom-forming group in the shelf COY

596 (Fig. 4), so the genus *Thalassiosira* might be capable of responding rapidly to environmental
597 changes such as an increase in temperature. Their rapid growth, however, was not observed in the
598 short-term incubation experiments. On the other hand, relative contributions of the genus
599 *Minidiscus* to the diatom assemblages increased at the Tokachi station (Bio-13) after the
600 temperature increase (Fig. 7). Because the physiological and phylogenic information on
601 *Minidiscus* were limited, further studies on this group are needed to understand their rapid
602 increase.

603 Among the other photosynthetic parameters from *P-E* curve analyses, α^B was considered to have
604 little variation with temperature because α^B is an index for the capability of carbon fixation in
605 light-limited environments and, thus, reflects mainly the light-dependent reactions of
606 photosynthesis (Platt and Jassby, 1976; Kiefer and Reynolds, 1992; Kolber and Falkowski, 1993).
607 In the incubation experiments at Stations Bio-7 and Bio-13, however, increases in α^B values were
608 observed with temperature (Fig. 8a). Although similar results were also observed in the previous
609 studies (e.g. Verity 1981; Palmisano et al., 1987), the mechanisms are still unclear. As estimated
610 from the small variations in F_v/F_{mPAM} (Fig. 8h), temperature negligibly affected the maximum
611 quantum yield of PSII for the phytoplankton assemblages at all stations in this study, but the light-
612 harvesting property of PSII could be affected by temperature. Because α^B values relate to σ_{PSII}
613 and the number of photosynthetic antennae (n) with varying non-photochemical quenching (e.g.,

614 Sakshaug et al., 1997), temperature might affect the light harvesting property of PSII i.e., *n* and

615 σ_{PSII} (e.g., Mock and Hoch, 2005; Ralph et al., 2005).

616

617 Acknowledgments

618 The authors are grateful to Dr. J. Nishioka for ship board assistance, nutrient analysis, and his

619 valuable comments. Dr. T. Hirawake is thanked for sharing his data on surface PAR and primary

620 productivity. We wish to acknowledge Mr. Weichen Qiu for his assistance in the 77 K

621 fluorescence measurements. Thanks are also extended to the officers and crew of R/V *Hakuho-*

622 *Maru* and TR/V *Misago-Maru*. This study was partly supported by the JSPS Grants-in-Aid for

623 Scientific Research (A) (JP17H00775) and (B) (JP18H03352). O.P. and E.L. were partly

624 supported by projects Algatech (CZ.1.05/2.1.00/03.0110) and Algatech Plus (MSMT LO 1416).

625

626 References

627

628 Abe, Y., Yamaguchi, A., Matsuno, K., Kono, T., Imai, I., 2014. Short-term changes in the
629 population structure of hydromedusa *Aglantha digitale* during the spring phytoplankton
630 bloom in the Oyashio region. Bull. Fish. Scicence, Hokkaido Univ. 64, 71–81.
631 Babin, M., Stramski, D., 2002. Light absorption by aquatic particles in the near-infrared spectral
632 region. Limnol. Oceanogr. 47, 911–915.
633 Behrenfeld, M.J. 2010. Abandoning Sverdrup's Critical Depth Hypothesis on phytoplankton
634 blooms. Ecology 91, 977–989.
635 Behrenfeld, M.J., Prasil, O., Babin, M., Bruyant, F., 2004. In search of a physiological basis for
636 covariations in light-limited and light-saturated photosynthesis. J. Phycol. 40, 4–25.
637 Behrenfeld, M.J., Randerson, J.T., McClain, C.R., Feldman, G.C., Los, S.O., Tucker, C.J.,

638 Falkowski, P.G., Field, C.B., Frouin, R., Esaias, W.E., Kolber, D.D., Pollack, N.H., 2001.
639 Biospheric primary production during an ENSO transition. Science 291, 2594–2597.
640 Chiba, S., Ono, T., Tadokoro, K., Midorikawa, T., Saino, T., 2004. Increased stratification and
641 decreased lower trophic level productivity in the Oyashio Region of the North Pacific: A
642 30-year retrospective study. J. Oceanogr. 60, 149–162.
643 Cleveland, J.S., Weidemann, A.D., 1993. Quantifying absorption by aquatic particles: A
644 multiple scattering correction for glass-fiber filters. Limnol. Oceanogr. 38, 1321–1327.
645 Crafts-Brandner, S.J., Salvucci, M.E., 2000. Rubisco activase constrains the photosynthetic
646 potential of leaves at high temperature and CO_2. Proc. Natl. Acad. Sci. U. S. A. 97, 13430–
647 13435.
648 Descolas-Gros, C., de Billy, G., 1987. Temperature adaptation of RuBP carboxylase: kinetic
649 properties in marine Antarctic diatoms. J. Exp. Mar. Bio. Ecol. 108, 147–158.
650 D'Haene, S.E., Sobotka, R., Bučinská, L., Dekker, J.P., Komenda, J., 2015. Interaction of the PsbH
651 subunit with a chlorophyll bound to histidine 114 of CP47 is responsible for the red 77K
652 fluorescence of Photosystem II. Biochim. Biophys. Acta. 1847, 1327-1334.
653 Endo, H., Sugie, K., Yoshimura, T., Suzuki, K., 2015. Effects of CO_2 and iron availability on
654 *rbcL* gene expression in Bering Sea diatoms. Biogeosciences 12, 2247–2259.
655 Endo, H., Sugie, K., Yoshimura, T., Suzuki, K., 2016. Response of spring diatoms to CO_2
656 availability in the western North Pacific as determined by next-generation sequencing.
657 PLoS One 11, e0154291.
658 Endo, H., Yoshimura, T., Kataoka, T., Suzuki, K., 2013. Effects of CO_2 and iron availability on
659 phytoplankton and eubacterial community compositions in the northwest subarctic Pacific.
660 J. Exp. Mar. Bio. Ecol. 439, 160–175.
661 Eppley, R.W., 1972. Temperature and phytoplankton growth in the sea. Fish. Bull. 70, 1063–
662 1085.
663 Falkowski, P.G., 1994. The role of phytoplankton photosynthesis in global biogeochemical
664 cycles. Photosynth. Res. 39, 235–258.
665 Field, C.B., Behrenfeld, M.J., Rnaderson, J.T., Falkowski, P.G., 1998. Primary production of
666 the biosphere: integrating terrestrial and oceanic components. Science 281, 237–240.
667 Hama, T., Miyazaki, T., Ogawa, Y., Iwakuma, T., Takahashi, M., Otsuki, A., Ichimura, S.,
668 1983. Measurement of photosynthetic production of a marine phytoplankton population
669 using a stable ^{13}C isotope. Mar. Biol. 73, 31–36.
670 Hasle G.R., Syvertsen E.E., Marine Diatoms, in: Tomas C.R. (Ed.), Identifying Marine
671 Phytoplankton. Academic Press, San Diego, pp. 5-386
672 Hattori-Saito, A., Nishioka, J., Ono, T., McKay, R.M.L., Suzuki, K., 2010. Iron deficiency in
673 micro-sized diatoms in the Oyashio region of the western subarctic Pacific during spring.

674 J. Oceanogr. 66, 105–115.
675 Hill, R., Larkum, A.W.D., Prášil, O., Kramer, D.M., Szabó, M., Kumar, V., Ralph, P.J., 2012.
676 Light-induced dissociation of antenna complexes in the symbionts of scleractinian corals
677 correlates with sensitivity to coral bleaching. Coral Reefs. 31, 963-975.
678 Honda, M.C., 2003. Biological pump in northwestern North Pacific. J. Oceanogr. 59, 671–684.
679 Hooker, S.B., Morrow, J.H., Matsuoka, A., 2013. Apparent optical properties of the Canadian
680 Beaufort Sea – Part 2: The 1 % and 1 cm perspective in deriving and validating AOP data
681 products. Biogeosci. 10, 4511–4527.
682 Hooker, S.B., 2014. Mobilization Protocols for Hybrid Sensors for Environmental AOP sampling
683 (HySEAS) Observations. NASA Tech. Pub. 2014−217518, NASA Goddard Space Flight
684 Center, Greenbelt, Maryland, 105pp.
685 Ikeda, T., Shiga, N., Yamaguchi, A., 2008. Structure, biomass distribution and trophodynamics
686 of the pelagic ecosystem in the Oyashio region, western subarctic Pacific. J. Oceanogr. 64,
687 339–354.
688 Isada, T., Hattori-Saito, A., Saito, H., Ikeda, T., Suzuki, K., 2010. Primary productivity and its
689 bio-optical modeling in the Oyashio region, NW Pacific during the spring bloom 2007.
690 Deep-Sea Res. II 57, 1653–1664.
691 Isada, T., Iida, T., Liu, H., Saitoh, S.I., Nishioka, J., Nakatsuka, T., Suzuki, K., 2013. Influence
692 of Amur River discharge on phytoplankton photophysiology in the Sea of Okhotsk during
693 late summer. J. Geophys. Res. Ocean 118, 1995–2013.
694 Isada, T., Kuwata, A., Saito, H., Ono, T., Ishii, M., Yoshikawa-Inoue, H., Suzuki, K., 2009.
695 Photosynthetic features and primary productivity of phytoplankton in the Oyashio and
696 Kuroshio–Oyashio transition regions of the northwest Pacific. J. Plankton Res. 31, 1009–
697 1025.
698 Isoda, Y., Kishi, M.J., 2003. A summary of "coastal Oyashio" symposium (in Japanese). Bull.
699 Coast. Oceanogr. 41, 1–3.
700 John, D.E., Patterson, S.S., Paul, J.H., 2007. Phytoplankton-group specific quantitative
701 polymerase chain reaction assays for RuBisCO mRNA transcripts in seawater. Mar.
702 Biotechnol. 9, 747–759.
703 Kasai, H., Saito, H., Yoshimori, A., Taguchi, S., 1997. Variability in timing and magnitude of
704 spring bloom in the Oyashio region, the western subarctic Pacific off Hokkaido, Japan.
705 Fish. Oceanogr. 6, 118–129.
706 Kawakami, H., Honda, M.C., Matsumoto, K., Wakita, M., Kitamura, M., Fujiki, T., Watanabe,
707 S., 2015. POC fluxes estimated from ^{234}Th in late spring–early summer in the western
708 subarctic North Pacific. J. Oceanogr. 71, 311–324.
709 Kawakami, H., Yang, Y.L., Honda, M.C., Kusakabe, M., 2004. Particulate organic carbon

fluxes estimated from ^{234}Th deficiency in winters and springs in the northwestern North Pacific. Geochem. J. 38, 581–592.

Kiefer, D.A., Reynolds, R.A., 1992. Advances in understanding phytoplankton fluorescence and photosynthesis, in: Falkowski, P.G., Woodhead, A.D. (Eds.), Primary Productivity and Biogeochemical Cycles in the Sea. Springer Science & Business Media, New York, pp. 155–174.

Kirk, J.T.O. (ed.), 2010. Light and Photosynthesis in Aquatic Ecosystems, 3rd edition. Cambridge Univ. Press, New York, 622 pp.

Kishino, M., Takahashi, M., Okami, N., Ichimura, S., 1985. Estimation of the spectral absorption coefficients of phytoplankton in the sea. Bull. Mar. Sci. 37, 634–642.

Kolber, Z., Falkowski, P.G., 1993. Use of active fluorescence to estimate phytoplankton photosynthesis in situ. Limnol. Oceanogr. 38, 1646–1665.

Kolber, Z., Prášil, O., Falkowski, P.G., 1998. Measurements of variable chlorophyll fluorescence using fast repetition rate techniques: defining methodology and experimental protocols. Biochim. Biophys. Acta 1367, 88–106.

Kono, T., 1997. Modification of the Oyashio Water in the Hokkaido and Tohoku areas. Deep-Sea Res. I 44, 669–688.

Kono, T., Foreman, M., Chandler, P., Kashiwai, M., 2004. Coastal Oyashio south of Hokkaido, Japan. J. Phys. Oceanogr. 34, 1477–1494.

Kono, T., Sato, M., 2010. A mixing analysis of surface water in the Oyashio region: Its implications and application to variations of the spring bloom. Deep-Sea Res. II 57, 1595–1607.

Kusaka, A., Azumaya, T., Kawasaki, Y., 2013. Monthly variations of hydrographic structures and water mass distribution off the Doto area, Japan. J. Oceanogr. 69, 295–312.

Li, W.K.W., Smith, J., Platt, T., 1984. Temperature response of photosynthetic capacity and carboxylase activity in Arctic marine phytoplankton. Mar. Ecol. Prog. Ser. 17, 237–243.

Liu, H., Suzuki, K., Nishioka, J., Sohrin, R., Nakatsuka, T., 2009. Phytoplankton growth and microzooplankton grazing in the Sea of Okhotsk during late summer of 2006. Deep-Sea Res. I 56, 561–570.

MacIntyre, H.L., Kana, T.M., Anning, T., Geider, R.J., 2002. Photoacclimation of photosynthesis irradiance response curves and photosynthetic pigments in microalgae and cyanobacteria. J. Phycol. 38, 17–38.

McQuoid, M.R., Godhe, A., 2004. Recruitment of coastal planktonic diatoms from benthic versus pelagic cells: Variations in bloom development and species composition. Limnol. Oceanogr. 49, 1123–1133.

Mochizuki, M., Shiga, N., Saito, M., Imai, K., Nojiri, Y., 2002. Seasonal changes in nutrients,

chlorophyll *a* and the phytoplankton assemblage of the western subarctic gyre in the Pacific Ocean. Deep-Sea Res. II 49, 5421-5439.

Mock, T., Hoch, N., 2005. Long-term temperature acclimation of photosynthesis in steady-state cultures of the polar diatom *Fragilariopsis cylindrus*. Photosynth. Res. 85, 307–317.

Monterey, G., Levitus, S, 1997. Seasonal variability of mixed layer depth for the world ocean. NOAA Atlas NESDIS 14, 100 pp.

Nishimura, A., Hamatsu, T., Yabuki, K., Shida, O., 2002. Recruitment fluctuations and biological responses of walleye pollock in the Pacific coast of Hokkaido. Fish. Sci. 68, 206–209.

Obayashi Y., Tanoue E., Suzuki K., Handa N., Nojiri Y., Wong C.S., 2001. Spatial and temporal variabilities of phytoplankton community structure in the northern North Paci"c as determined by phytoplankton pigments. Deep-Sea Res. I 48, 439-469

Ogasawara, J., 1990. Physics on the east and south coasts of Hokkaido (in Japanese), in: Kunishi, H. (Ed.), Coastal Oceanography of Japanese Islands. Tokai University Press, 839 pp.

Oguma, S., Ono, T., Kusaka, A., Kasai, H., Kawasaki, Y., Azumaya, T., 2008. Isotopic tracers for water masses in the coastal region of Eastern Hokkaido. J. Oceanogr. 64, 525–539.

Ohtani, K., 1971. Studies on the change of the hydrographic conditions in the Funka Bay PartII: Characteristics of the waters occupying the Funka Bay (in Japanese with English abstract). Bull. Fac. Fish. Hokkaido Univ. 22, 58–61.

Okamoto, S., Hirawake, T., Saitoh, S.-I., 2010. Interannual variability in the magnitude and timing of the spring bloom in the Oyashio region. Deep-Sea Res. II 57, 1608–1617.

Oxborough, K., Moore, C.M., Suggett, D.J., Lawson, T., Chan, H.G., Geider, R.J., 2012. Direct estimation of functional PSII reaction center concentration and PSII electron flux on a volume basis: a new approach to the analysis to Fast Repetition Rate fluorometry (FRRf) data. Limnol. Oceanogr. Methods 10, 142–154.

Palmisano, A.C., SooHoo, J.B., Sullivan, C.W., 1987. Effects of four environmental variables on photosynthesis-irradiance relationships in Antarctic sea-ice microalgae. Mar. Biol. 94, 299–306.

Platt, T., Gallegos, C.L., Harrison, W.G., 1980. Photoinibition of photosynthesis in natural assemblages of marine phytoplankton. J. Mar. Res. 38, 103–111.

Platt, T., Jassby, A.D., 1976. The relationship between photosynthesis and light for natural assemblages of coastal marine phytoplankton. J. Phycol. 12, 421–430.

Prášil, O., Bína, D., Medová, H., Řeháková, K., Zapomělová, E., Veselá, J., Oren E., 2009. Emission spectroscopy and kinetic fluorometry studies of phototrophic microbial communities along a salinity gradient in solar saltern evaporation ponds of Eilat, Israel.

Aquat. Microb. Ecol. 56, 285-296.
Ralph, P.J., McMinn, A., Ryan, K.G., Ashworth, C., 2005. Short-term effect of temperature on the photokinetics of microalgae from the surface layers of Antarctic pack ice. J. Phycol. 41, 763–769.
Raven, J.A., Geider, R.J., 1988. Temperature and algal growth. New Phytol. 110, 441–461.
Saito, H., Tsuda, A., 2003. Influence of light intensity on diatom physiology and nutrient dynamics in the Oyashio region. Prog. Oceanogr. 57, 251–263.
Saito, H., Tsuda, A., Kasai, H., 2002. Nutrient and plankton dynamics in the Oyashio region of the western subarctic Pacific Ocean. Deep-Sea Res. II 49, 5463–5486.
Sakshaug, E., Bricaud, A., Dandonneau, Y., Falkowski, P.G., Kiefer, D.A, Legendre, L., Morel, A., Parslow, J., Takahashi, M., 1997. Parameters of photosynthesis: definitions, theory and interpretation of results. J. Plankton Res. 19, 1637–1670.
Sakurai, Y., 2007. An overview of the Oyashio ecosystem. Deep-Sea Res. II 2526–2542.
Sarmiento, J.L., Siegenthaler, U., 1992. New production and the global carbon cycle, in: Falkowski, P.G., Woodhead, A.D. (Eds.), Primary Productivity and Biogeochemical Cycles in the Sea. Springer Science & Business Media, New York, pp. 317–332.
Schloss, P.D., Westcott, S.L., Ryabin, T., Hall, J.R., Hartmann, M., Hollister, E.B., Lesniewski, R.A., Oakley, B.B., Parks, D.H., Robinson, C.J., Sahl, J.W., Stres, B., Thallinger, G.G., Van Horn, D.J., Weber, C.F., 2009. Introducing mothur: Open-source, platform-independent, community-supported software for describing and comparing microbial communities. Appl. Environ. Microbiol. 75, 7537–7541.
Shinada, A., Shiga, N., Ban, S., 1999. Structure and magnitude of diatom spring bloom in Funka Bay, southwestern Hokkaido, Japan, as influenced by the intrusion of Coastal Oyashio Water. Plankton Biol. Ecol. 46, 24–29.
Smetacek, V., 1999. Diatoms and the ocean carbon cycle. Protist 150, 25–32.
Suggett, D.J., Stambler, N., Prášil, O., Kolber, Z., Quigg, A., Vázquez-Dominguez, E., Zohary, T., Berman, T., Iluz, D., Levitan, O., Lawson, T., Meeder, E., Lazar, B., Bar-Zeev, E., Medova, H., Berman-Frank, I., 2009. Nitrogen and phosphorus limitation of oceanic microbial growth during spring in the Gulf of Aqaba. Aquat. Microb. Ecol. 56, 227-239.
Sugiura, J., 1956. A Note on Current Branches in the Oyashio Area (in Japanese with English abstract). J. Oceanogr. Soc. Japan 12, 117–119.
Suzuki, K., Handa, N., Nishida, T., Wong, C.S., 1997. Estimation of phytoplankton succession in a fertilized mesocosm during summer using high-performance liquid chromatographic analysis of pigments. J. Exp. Mar. Biol. Ecol. 214, 1-17.
Suzuki, K., Kamimura, A., Hooker, S.B., 2015. Rapid and highly sensitive analysis of chlorophylls and carotenoids from marine phytoplankton using ultra-high performance

liquid chromatography (UHPLC) with the first derivative spectrum chromatogram (FDSC) technique. Mar. Chem. 176, 96–109.

Suzuki, K., Kuwata, A., Yoshie, N., Shibata, A., Kawanobe, K., Saito, H., 2011. Population dynamics of phytoplankton, heterotrophic bacteria, and viruses during the spring bloom in the western subarctic Pacific. Deep-Res. I 58, 575–589.

Suzuki, K., Liu, H., Saino, T., Obata, H., Takano, M., Okamura, K., Sohrin, Y., Fujishima, Y., 2002. East-west gradients in the photosynthetic potential of phytoplankton and iron concentration in the subarctic Pacific Ocean during early summer. Limnol. Oceanogr. 47, 1581–1594.

Suzuki, R., Ishimaru, T., 1990. An improved method for the determination of phytoplankton chlorophyll using N, N-dimethylformamide. J. Oceanogr. Soc. Japan 46, 190–194.

Takahashi, T., Sutherland, S.C., Sweeney, C., Poisson, A., Metzl, N., Tilbrook, B., Bates, N., Wanninkhof, R., Feely, R.A., Sabine, C., Olafsson, J., Nojiri, Y., 2002. Global sea-air CO_2 flux based on climatological surface ocean pCO_2, and seasonal biological and temperature effects. Deep-Sea Res. II 49, 1601–1622.

Taniguchi, A., 1999. Differences in the structure of the lower trophic levels of pelagic ecosystems in the eastern and western subarctic Pacific. Prog. Oceanogr. 43, 289–315.

Van Heukelem, L., Thomas, C.S., 2001. Computer-assisted high-performance liquid chromatography method development with applications to the isolation and analysis of phytoplankton pigments. J. Chromatogr. A 910, 31–49.

Verity, P.G., 1981. Effects of temperature, irradiance, and daylength on the marine diatom *Leptocylindrus danicus* Cleve. I. Photosynthesis and cellular composition. J. Exp. Mar. Bio. Ecol. 55, 79–91.

Welschmeyer, N.A., 1994. Fluorometric analysis of chlorophyll *a* in the presence of chlorophyll *b* and pheopigments. Limnol. Oceanogr. 39, 1985–1992.

Yamaguchi, A., Miwa, Y., Inoue, K., Matsumoto, T., 2003. Characteristics of zooplankton community in the coastal Oyahsio water (in Japanese with English abstract). Bull. Coast. Oceanogr. 41, 23–31.

Yasuda, I., 2003. Hydrographic structure and variability in the Kuroshio-Oyashio transition area. J. Oceanogr. 59, 389–402.

Yoshie, N., Suzuki, K., Kuwata, A., Nishioka, J., Saito, H., 2010. Temporal and spatial variations in photosynthetic physiology of diatoms during the spring bloom in the western subarctic Pacific. Mar. Ecol. Prog. Ser. 399, 39–52.

Yoshie, N., Yamanaka, Y., Kishi, M.J., Saito, H., 2003. One dimensional ecosystem model simulation of the effects of vertical dilution by the winter mixing on the spring diatom bloom. J. Oceanogr. 59, 563–571.

Yoshimori, A., Ishizaka, J., Kono, T., Kasai, H., Saito, H., Kishi, M.J., Taguchi, S., 1995. Modeling of spring bloom in the western subarctic Pacific (off Japan) with observed vertical density structure. J. Oceanogr. 51, 471–488.

Young, J.N., Goldman, J.A.L., Kranz, S.A., Tortell, P.D., Morel, F.M.M., 2015. Slow carboxylation of Rubisco constrains the rate of carbon fixation during Antarctic phytoplankton blooms. New Phytol. 205, 172–181.

Figure captions

Figure 1. Seawater sampling stations during the KH15-1 and AK15 expeditions off the coast of Hokkaido, Japan. Stations for the KH15-1 expedition are denoted as B plus station numbers. Stations Bio-6, Bio-7, and Bio-11 overlap as well as stations AK15-1 and AK15-2. Red circles denote shelf COY stations, blue circles denote offshore COY stations, and green closed denote Tokachi stations.

Figure 2. Photosynthetic parameters obtained from *P-E* curve experiments at *in situ* sampling stations.
Chl *a*: Chl *a* concentration [mg m^{-3}]; F_v/F_{mPAM}: Maximum quantum yield of PSII obtained by PAM fluorometry; $\bar{a}^*_{ph}$: Chl *a*-normalized light absorption coefficient of phytoplankton [m^2 mg Chl *a*]; α^B: Initial slope of *P-E* curve [mg C mg Chl a^{-1} h^{-1} (μmol photons m^{-2} s^{-1}) $^{-1}$]; β^B: Photoinhibition index [mg C mg Chl a^{-1} h^{-1} (μmol photons m^{-2} s^{-1}) $^{-1}$]; P^B_{max}: Maximum photosynthetic rate [mgC mgChl a^{-1} h^{-1}]; E_k: Light saturation index [μmol photons m^{-2} s^{-1}]; Φ_{Cmax}: Maximum quantum yield for carbon fixation [mol C mol photons^{-1}]; *PP*: Primary productivity [mg C m^{-3} day^{-1}]. Error bars are standard deviations, $n \geq 3$.

Figure 3. Relative contribution of phytoplankton groups to total Chl *a* (a) at the class level class at the different sampling stations determined by multiple regression analysis based on diagnostic pigment signatures and (b) at the level of size class of phytoplankton determined by size-fractioned Chl *a* measurement.

Figure 4. Relative contribution of diatom community composition to total number of sequences determined by the next-generation sequencing method at *in situ* sampling stations.

Figure 5. Dendrogram of the cluster analysis of diatom community composition determined with the next-generation sequencing method. Clustering is based on Bray-Curtis distance and the group average method. The cluster on the right-hand side includes samples from shelf COY water, which had a community composition significantly different from the other sites (One- way MANOVA, Wilk's lambda, $p < 0.01$).

Figure 6. Relative contribution of phytoplankton groups to total Chl *a* at the class level during the temperature-controlled incubation experiments determined by the multiple regression analysis based on diagnostic pigments.

Figure 7. Relative contribution of diatom community composition to total number of sequences during the temperature-controlled incubation experiments determined with the next-generation sequencing method.

Figure 8. Photosynthetic parameters during the temperature-controlled incubation experiments. The open bars indicate values of initial bottles, shaded bars indicate values of control treatments, and closed bars show values of the +7 ºC treatment.
(a) α^{B}: Initial slope of *P-E* curve [mg C mg Chl a^{-1} h^{-1} (μmol photons m^{-2} s^{-1}) $^{-1}$]; (b) β^{B}: Photoinhibition index [mg C mg Chl a^{-1} h^{-1} (μmol photons m^{-2} s^{-1}) $^{-1}$]; (c) P^{B}_{max}: Maximum photosynthetic rate [mgC mgChl a^{-1} h^{-1}]; (d) E_k: Light saturation index [μmol photons m^{-2} s^{-1}]; (e) $\bar{a}^*_{ph}$: Chl *a*-normalized light absorption coefficient of phytoplankton [m^2 mg Chl *a*]; (f) Φ_{Cmax}: Maximum quantum yield for carbon fixation [mol C mol photons^{-1}]; (g) Diatom-specific *rbcL*: Transcription level of the diatom-specific *rbcL* gene (cDNA copies/DNA copies); (h) F_v/F_{mPAM}: Maximum quantum yield of PSII obtained by PAM fluorometry. Error bars are standard deviations, $n \geq 3$.

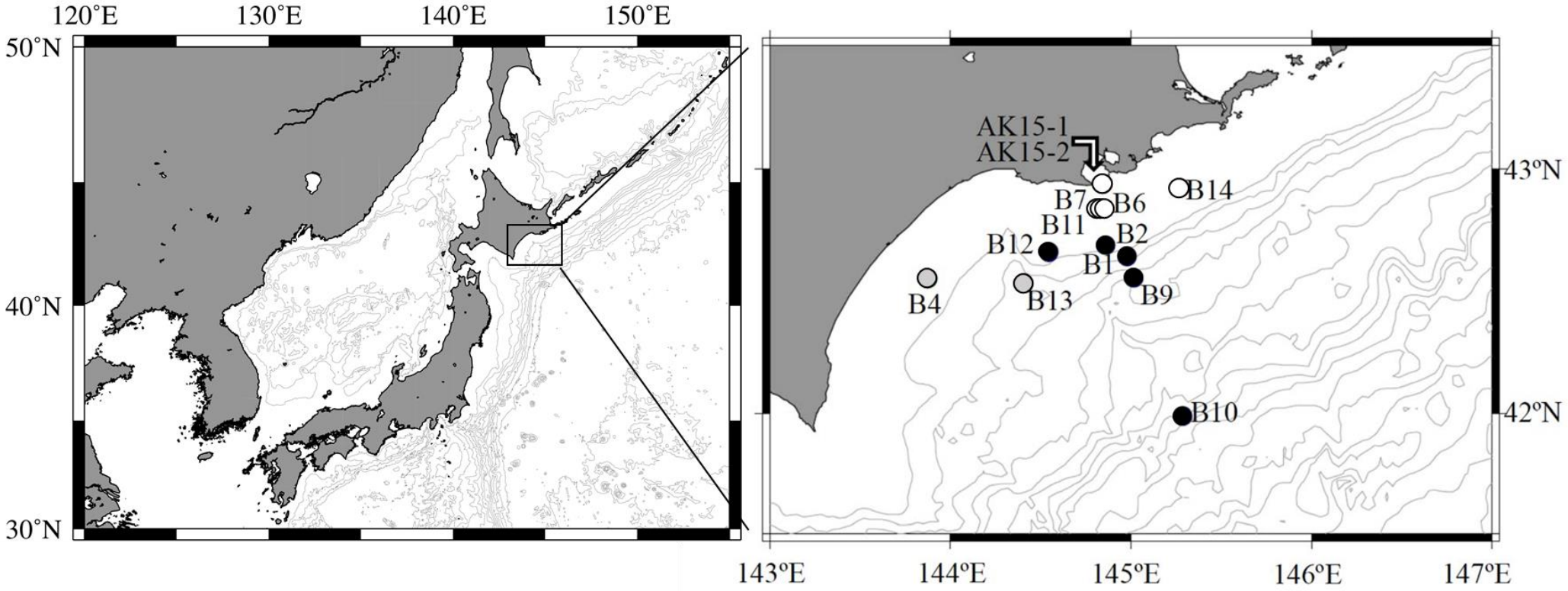
120°E
130°E
140°E
150°E
50°N
40°N
30°N
AK15-1
AK15-2
B14
B7
B6
B11
B2
B12
B1
B4
B13
B9
B10
43°N
42°N
143°E
144°E
145°E
146°E
147°E

Fig. 1

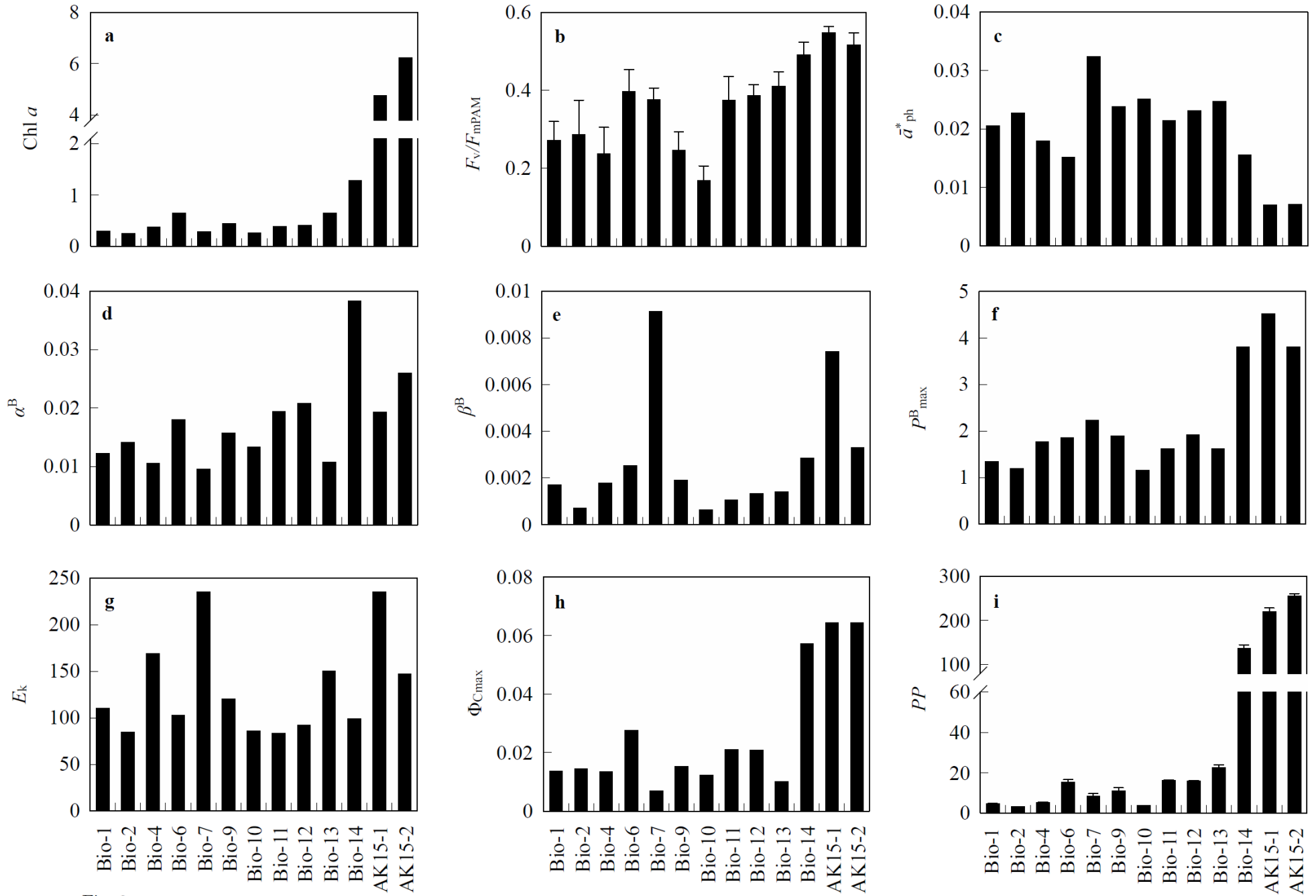
a
Chl a
b
F_v/F_{mPAM}
c
$\vec{a}^*_{ph}$
d
α^B
e
β^B
f
P^B_{max}
g
E_k
h
Φ_{Cmax}
i
PP
Bio-1
Bio-2
Bio-4
Bio-6
Bio-7
Bio-9
Bio-10
Bio-11
Bio-12
Bio-13
Bio-14
AK15-1
AK15-2

Fig. 2

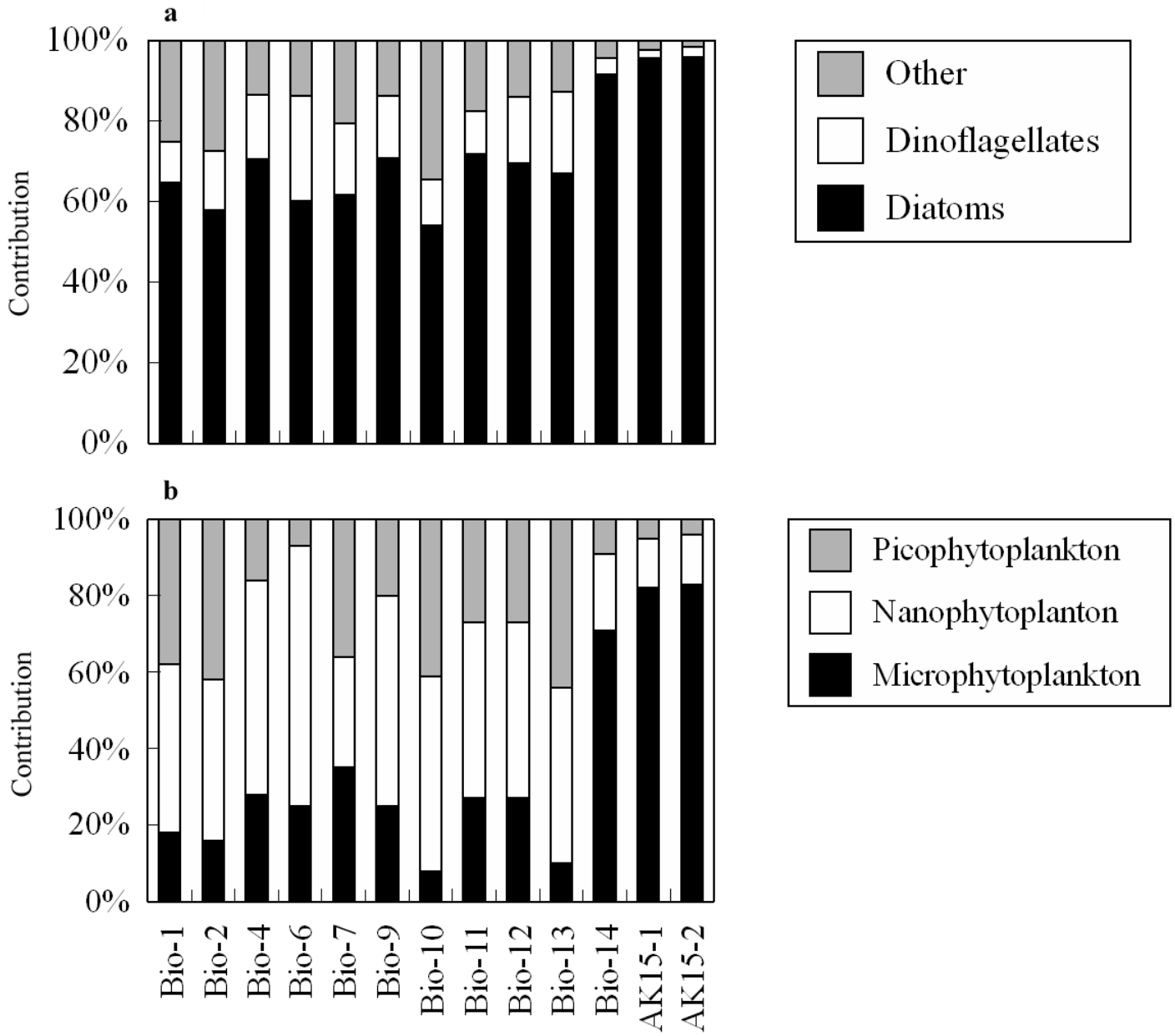
a
100%
80%
60%
40%
20%
0%
Contribution
Other
Dinoflagellates
Diatoms
b
100%
80%
60%
40%
20%
0%
Contribution
Picophytoplankton
Nanophytoplanton
Microphytoplankton
Bio-1
Bio-2
Bio-4
Bio-6
Bio-7
Bio-9
Bio-10
Bio-11
Bio-12
Bio-13
Bio-14
AK15-1
AK15-2

Fig. 3

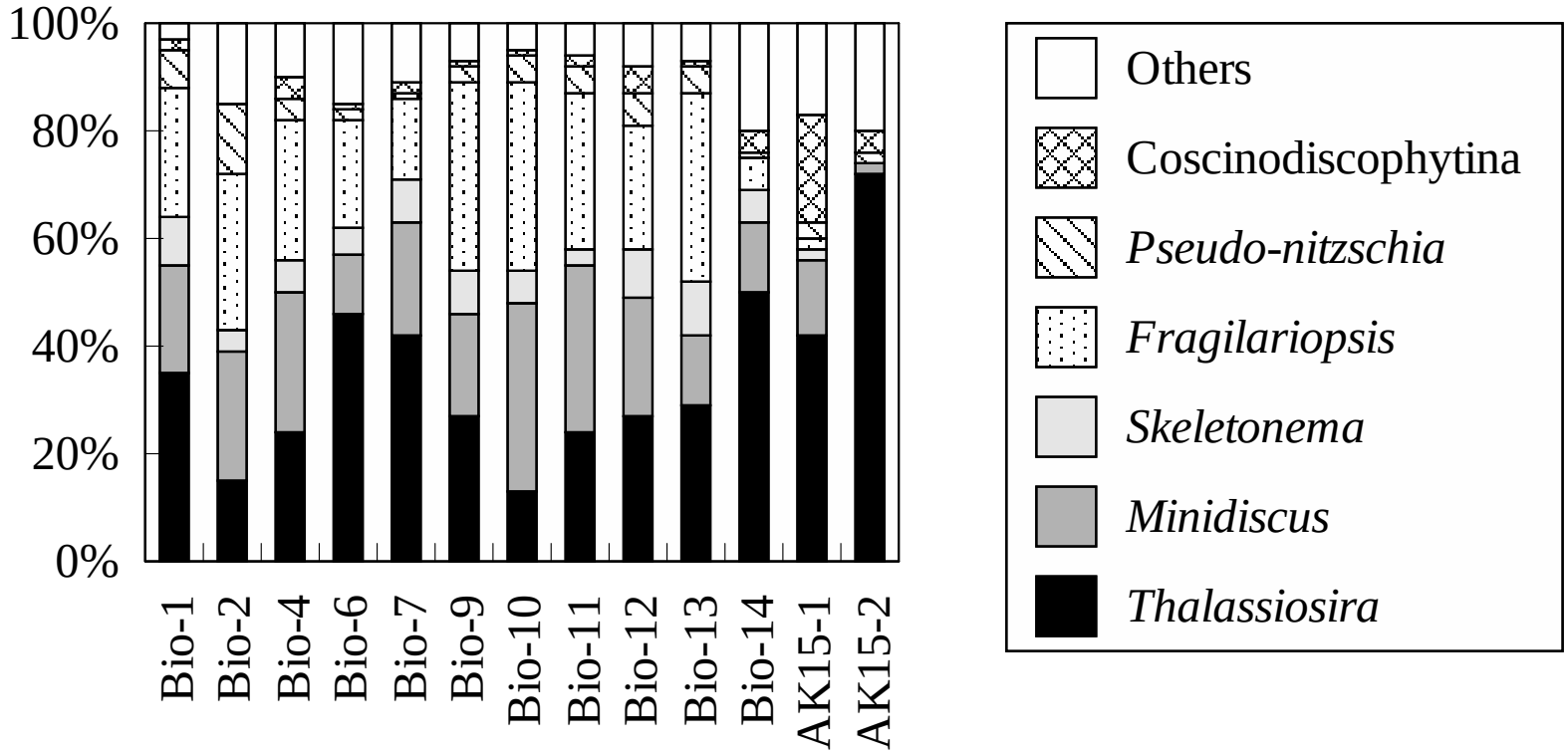
100%
80%
60%
40%
20%
0%
Bio-1
Bio-2
Bio-4
Bio-6
Bio-7
Bio-9
Bio-10
Bio-11
Bio-12
Bio-13
Bio-14
AK15-1
AK15-2
Others
Coscinodiscophytina
Pseudo-nitzschia
Fragilariopsis
Skeletonema
Minidiscus
Thalassiosira

Fig. 4

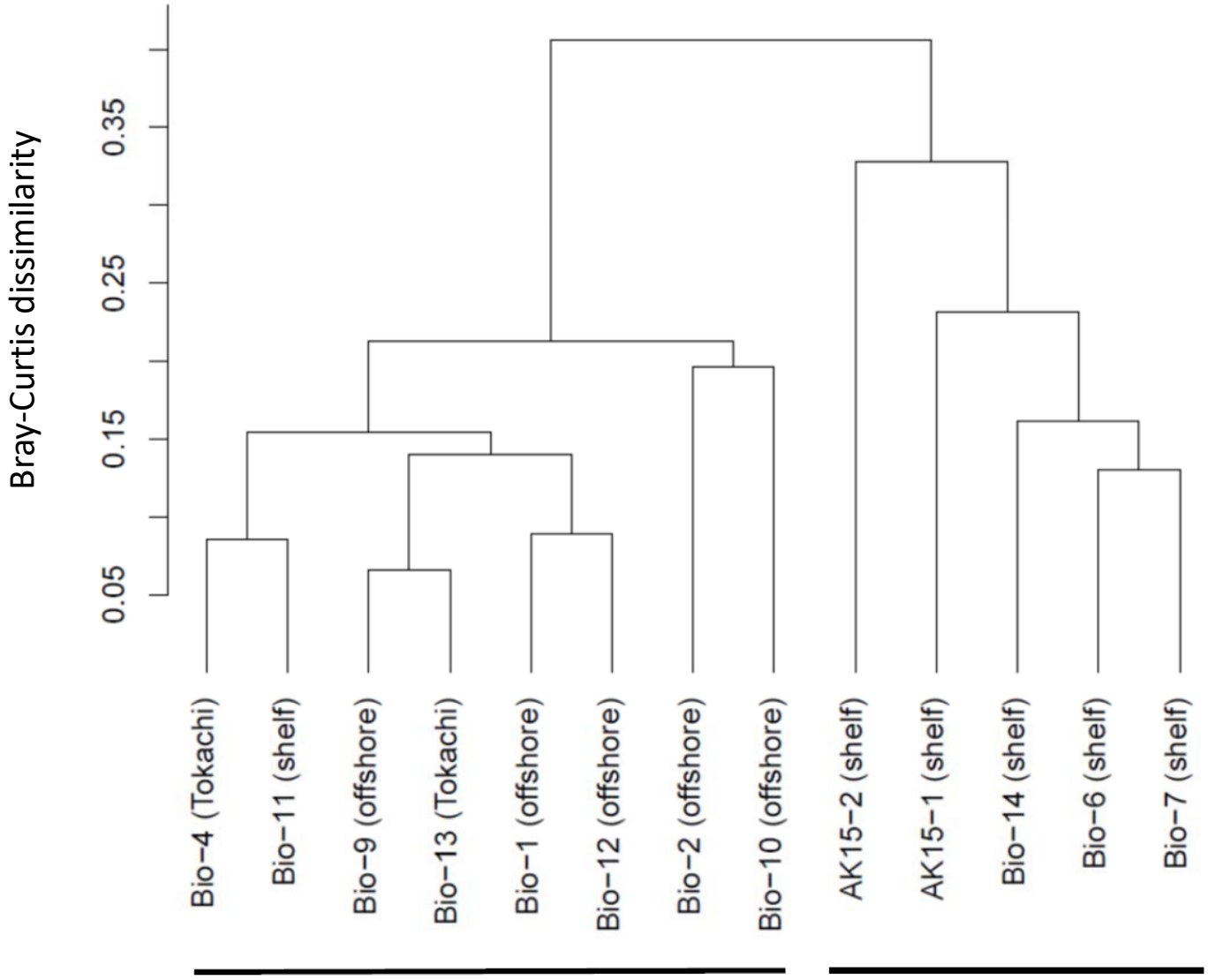
Bray-Curtis dissimilarity
0.05
0.15
0.25
0.35
Bio−4 (Tokachi)
Bio−11 (shelf)
Bio−9 (offshore)
Bio−13 (Tokachi)
Bio−1 (offshore)
Bio−12 (offshore)
Bio−2 (offshore)
Bio−10 (offshore)
AK15−2 (shelf)
AK15−1 (shelf)
Bio−14 (shelf)
Bio−6 (shelf)
Bio−7 (shelf)

Fig. 5

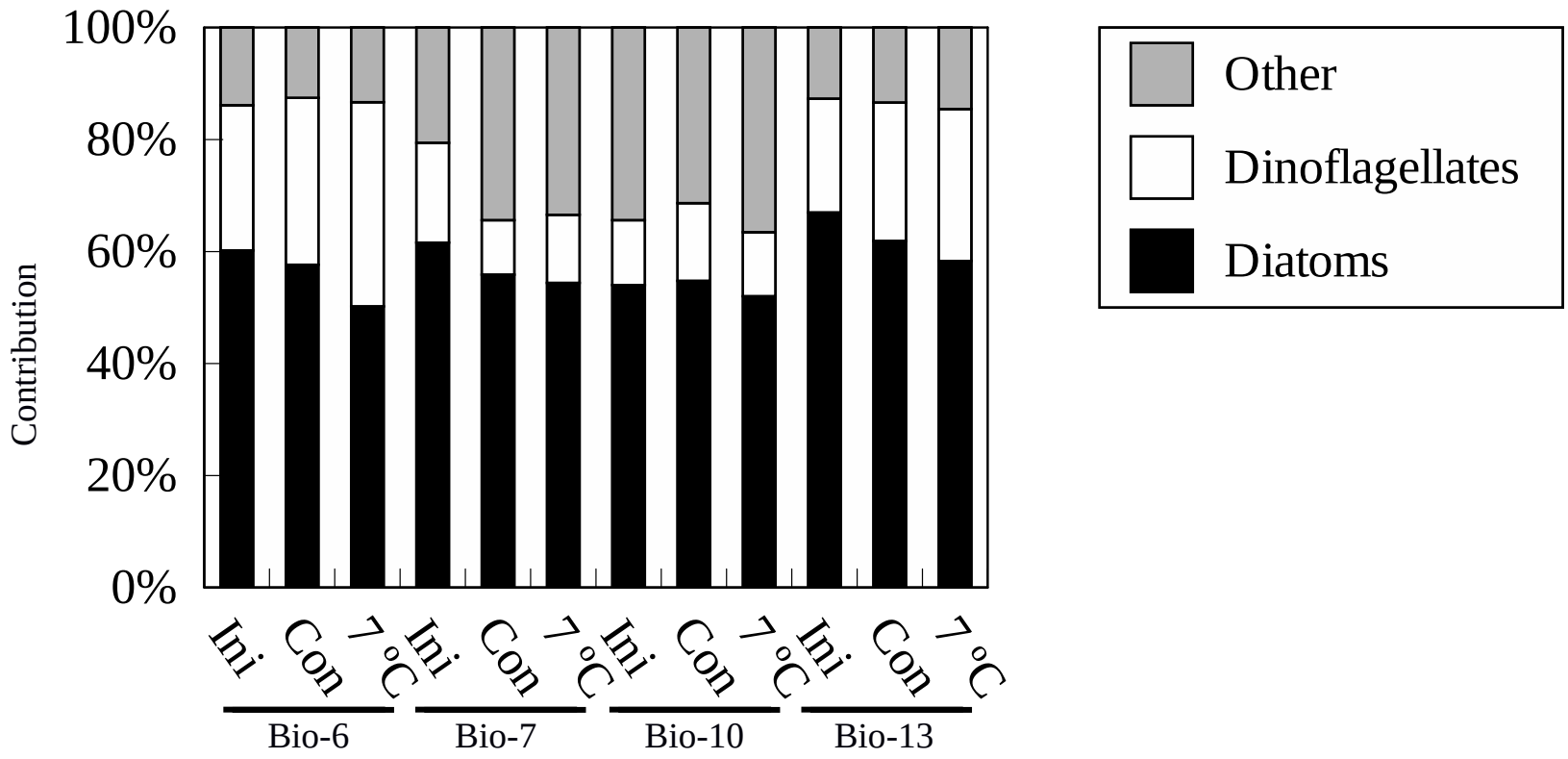
100%
80%
60%
40%
20%
0%
Contribution
Ini
Con
7 °C
Bio-6
Bio-7
Bio-10
Bio-13
Other
Dinoflagellates
Diatoms

Fig. 6

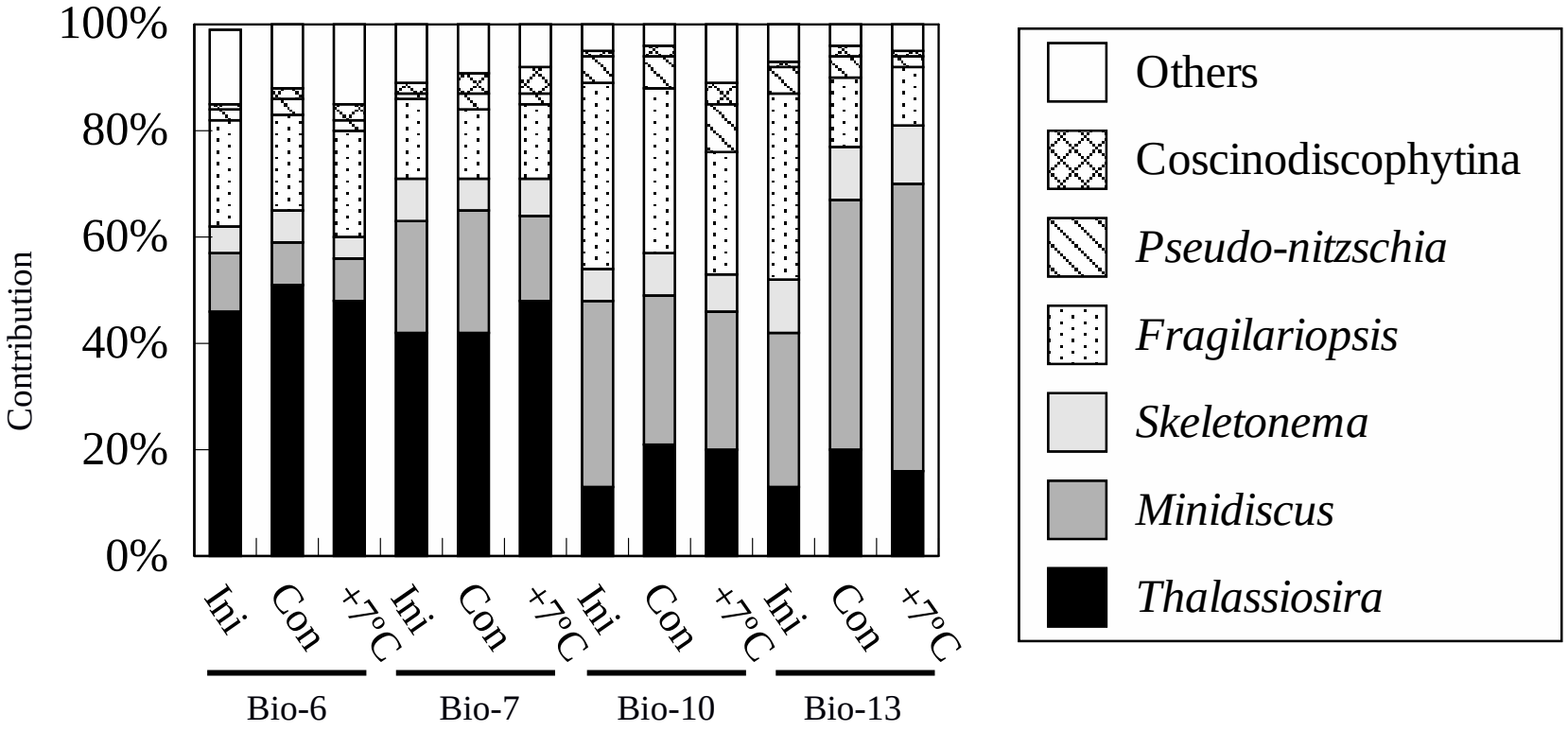
100%
80%
60%
40%
20%
0%
Contribution
Ini
Con
+7°C
Bio-6
Bio-7
Bio-10
Bio-13
Others
Coscinodiscophytina
Pseudo-nitzschia
Fragilariopsis
Skeletonema
Minidiscus
Thalassiosira

Fig. 7

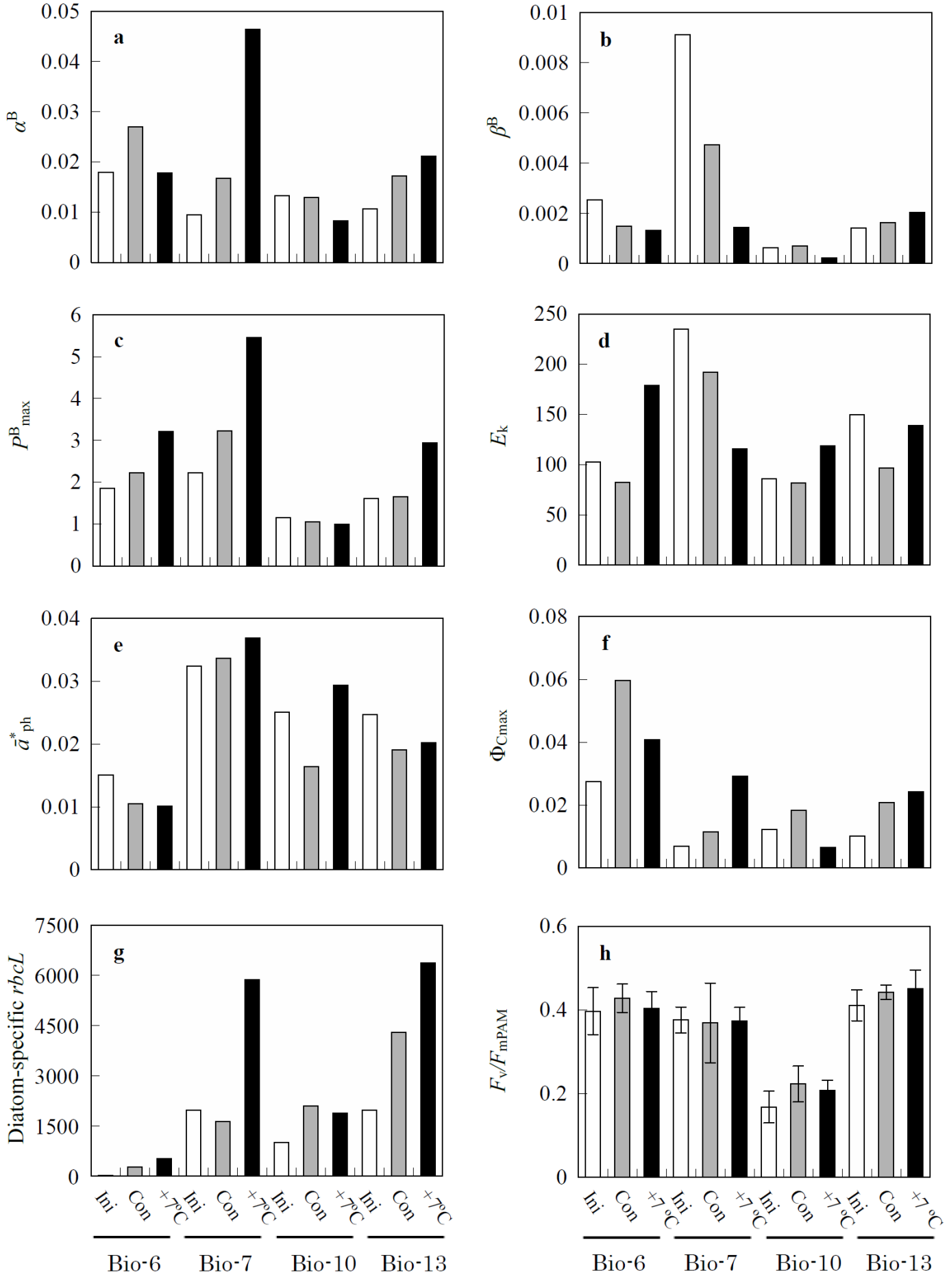
a
b
c
d
e
f
g
h
α^B
β^B
P^B_{max}
E_k
$\bar{a}^*_{ph}$
Φ_{Cmax}
Diatom-specific *rbcL*
F_v/F_{mPAM}
Ini
Con
+7°C
+7 °C
Bio-6
Bio-7
Bio-10
Bio-13

Fig. 8

Table captions

Table 1. Sampling conditions and hydrographic and optical data during the KH15-1 and AK15 expeditions.
SST: Sea surface temperature; SSS: Sea surface salinity; NO_3, NO_2, NH_4, PO_4, and SiO_2: Concentration of nitrate, nitrite, ammonium, phosphate, and silicate; K_d(PAR): Vertical attenuation coefficient of downward photosynthetically available radiation (PAR); Z_{eu}: Euphotic layer depth; MLD: Mixed layer depth

Table 2. Spearman-rank correlation coefficients between photosynthetic, environmental and community composition data.
Bold values indicate significant relationships with asterisks denoting different significance levels: * = 0.05, ** = 0.01, *** = 0.001, n = 13
SST: Sea surface temperature; SSS: Sea surface salinity; NO_3, NO_2, NH_4, PO_4, and SiO_2: Concentration of nitrate, nitrite, ammonium, phosphate, and silicate; MLD: Mixed layer depth; *rbcL*: Diatom-specific *rbcL* gene expression, Micro: microphytoplankton, Nano: nanophytoplankton, Pico: Picophytoplankton, Dino: dinoflagellates, Other: other functional groups than diatoms and dinoflagellates. The % denotes relative contribution of given phytoplankton groups.

Table 3. Spearman-rank correlation coefficients between *P-E* curve parameters.
Bold numbers indicate significant relationship between given parameters. Significance levels are denoted by numbers of asterisks: * = 0.05, ** = 0.01, *** = 0.001, n = 13.
α^B: Initial slope of *P-E* curve [mg C mg Chl a^{-1} h^{-1} (μmol photons m^{-2} s^{-1}) $^{-1}$]; β^B: Photoinhibition index [mg C mg Chl a^{-1} h^{-1} (μmol photons m^{-2} s^{-1}) $^{-1}$]; P^B_{max}: Maximum photosynthetic rate [mgC mgChl a^{-1} h^{-1}]; E_k: Light saturation index [μmol photons m^{-2} s^{-1}]; Chl *a*: Chl *a* concentration [mg m^{-3}]; $\bar{a}^*_{ph}$: Chl *a*-normalized light absorption coefficient of phytoplankton [m^2 mg Chl *a*]; Φ_{Cmax}: Maximum quantum yield for carbon fixation [mol C mol photons^{-1}]; *PP*: Primary productivity [mg C m^{-3} day^{-1}]

Table 1

Sampling date	Station	Water mass	Bottom depth (m)	SST (°C)	SSS	NO_3 (μM)	NO_2 (μM)	NH_4 (μM)	PO_4 (μM)	SiO_2 (μM)	K_d(PAR) (m^{-1})	Z_{eu} (m)	MLD (m)
2015.03.08	Bio-1	Offshore	852	0.03	32.58	21.29	0.18	0.69	1.81	35.50	0.105	44.1	26.6
2015.03.09	Bio-2	Offshore	564	0.39	32.71	22.20	0.11	0.44	1.93	35.38	0.12	38.5	29.9
2015.03.13	Bio-4	Tokachi	103	0.42	32.36	18.43	0.23	0.71	1.71	33.73	0.291	15.8	27.3
2015.03.14	Bio-6	Shelf	100	0.93	32.17	19.77	0.18	1.43	1.54	39.24	0.363	12.7	15.8
2015.03.15	Bio-7	Shelf	97	0.67	32.55	20.64	0.18	1.02	1.85	36.25	0.145	31.7	20.2
2015.03.17	Bio-9	Offshore	1477	0.64	32.38	18.13	0.23	0.54	1.76	32.19	0.159	28.9	19.5
2015.03.18	Bio-10	Offshore	4100	1.60	32.78	24.70	0.17	UD	2.21	43.22	0.087	52.6	28.6
2015.03.19	Bio-11	Shelf	100	0.85	32.71	23.60	0.16	0.27	2.10	41.01	0.119	38.9	20.1
2015.03.20	Bio-12	Offshore	529	0.63	32.62	27.21	0.21	0.35	2.45	48.93	0.137	33.9	23.6
2015.03.21	Bio-13	Tokachi	1084	1.47	32.62	24.53	0.27	0.29	2.30	46.03	0.131	35.0	18.9
2015.03.22	Bio-14	Shelf	100	0.56	32.52	31.43	0.33	0.27	2.94	59.28	0.143	32.1	19.5
2015.04.16	AK15-1	Shelf	33	3.84	32.06	0.83	0.05	UD	0.34	4.12	ND	ND	27.8
2015.04.17	AK15-2	Shelf	32	2.41	32.22	2.01	0.08	UD	0.48	1.78	ND	ND	21.4

Table 2

	Chl *a*	$F_v/F_{m\ PAM}$	α^B	β^B	P^B_{MAX}	E_k	$\bar{a}^*_{ph}$	Φ_{cm}	PP
SST	**0.57***	0.52	0.22	0.27	0.35	0.26	–0.14	0.28	**0.57***
SSS	**–0.66***	–0.50	–0.20	**–0.83*****	**–0.76****	**–0.65***	**0.70****	–0.55	–0.50
NO_3	–0.29	–0.13	0.12	**–0.57***	–0.48	**–0.60***	0.45	–0.20	–0.17
NO_2	0.08	–0.10	–0.14	–0.03	–0.08	0.07	0.28	–0.32	–0.04
NH_4	–0.36	–0.33	–0.51	0.15	–0.15	0.20	0.19	–0.41	–0.45
PO_4	–0.26	–0.13	0.08	–0.52	–0.33	–0.51	**0.56***	–0.34	–0.12
SiO_2	–0.12	0.00	0.11	–0.30	–0.25	–0.43	0.39	–0.23	–0.03
MLD	–0.49	–0.32	–0.15	–0.31	–0.24	–0.12	–0.02	–0.09	–0.44
rbcL	0.41	0.29	0.19	0.15	0.33	0.27	0.00	0.20	0.47
%Micro	**0.57***	**0.61***	0.46	**0.77****	**0.91*****	0.44	**–0.59***	**0.59***	**0.66***
%Nano	–0.31	–0.63*	–0.33	–0.44	–0.53	–0.23	0.28	–0.35	–0.47
%Pico	**–0.69***	**–0.49**	**–0.58***	**–0.60***	**–0.77****	–0.27	**0.80****	**–0.80****	**–0.61***
%Diatom	**0.61***	0.40	0.53	0.34	0.54	0.17	**–0.57***	**0.61***	0.64*
%Dino	–0.35	–0.22	–0.52	–0.19	–0.35	0.04	0.52	–0.59*	–0.30
%*Thalassiosira*	**0.70***	**0.76****	0.34	**0.84*****	**0.74****	0.48	–0.51	0.47	**0.65***
%*Minidiscus*	–0.80	**–0.75****	–0.37	**–0.67***	**–0.59***	–0.39	0.52	–0.51	**–0.66***
%*Skeletonema*	–0.21	–0.29	–0.45	–0.17	–0.25	0.17	0.60*	**–0.64***	–0.27
%*Fragilariopsis*	–0.45	**–0.65***	–0.45	**–0.73****	**–0.77****	–0.32	**0.65***	**–0.61***	–0.49
%*Pseudo-Nitzschia*	–0.45	–0.41	–0.18	**–0.83*****	**–0.72****	–0.50	0.25	–0.29	–0.47
%Coscinodiscophytina	0.52	0.53	0.53	0.42	**0.69****	0.21	**–0.59***	**0.58***	**0.62***

Table 3

	Chl *a*	$\bar{a}^*_{ph}$	F_v/F_{mPAM}	α^B	β^B	P^B_{max}	E_k	Φ_{Cmax}
F_v/F_{mPAM}	**0.80****	–						
$\bar{a}^*_{ph}$	**–0.62***	–0.53	–					
α^B	0.60*	0.54	–0.55	–				
β^B	**0.56***	**0.58***	–0.40	0.09	–			
P^B_{max}	**0.72****	**0.72****	–0.48	0.50	**0.84*****	–		
E_k	0.33	0.28	–0.09	–0.42	**0.75****	0.51	–	
Φ_{Cmax}	**0.69***	**0.62****	**–0.83*****	**0.87*****	0.34	**0.61***	–0.15	–
PP	**0.92*****	**0.88*****	–0.53	**0.64***	0.52	**0.75****	0.25	**0.68****

Appendices

Appendix A. Potential temperature *(θ)* between the isopycnal surfaces σ_θ = 26.7 and 26.8 at all sampling stations.

Appendix B. Pigment composition determined with the UHPLC analysis method (Suzuki et al., 2015) at all stations.
Chl: chlorophyll, Chlide: chlorophilide, Peri: peridinin, 19'-BF: 19'-butanoyloxyfucoxanthin, Fuco: fucoxanthin, Neo: neoxanthin, Prasino: prasinoxanthin, Viola: violaxanthin, 19'-HF: 19'-hexanoyloxyfucxanthin, DD: diadinoxanthin, Allo: alloxanthin, DT: diatoxanthin, Zea: zeaxanthin, Lut: lutein, Caro: carotene

Appendix C. FRRf parameters obtained at all sampling stations ± standard deviations, n = 2.
F_v/F_{mFRRf}: Maximum quantum yield of PSII obtained by FRR fluorometer. σ_{PSII}:
Functional absorption cross-section for PSII
[RCII]: Concentration of functional PSII reaction center

Appendix D. Low temperature (77K) emission spectra. Panels A and B show part of the emission in the range 660-700nm of selected samples from different stations. (A) shows spectra excited by 390 nm, (B) shows spectra excited at 530 nm. The arrows and lines indicate the positions of individual emission bands (675, 680, 685, 695 nm). (C) shows relationship between the relative content of peridinin (% of all pigments) and the increase of the 675 nm emission when excited at 530 nm (calculated as difference between emission at 675 nm when excited at 530 and 390 nm). (D) shows the relationship between PSII effective cross-section (σ_{PSII}) and the emission band intensity at 678nm when excited at 390 nm.

Appendix E. A relationship between F_v/F_{mPAM} and F_v/F_{mFRRf}.
The parameters were significantly correlated each other (ρ=0.483, n=20, p<0.05, Spearman's Rank correlation)
F_v/F_{mPAM}: Maximum quantum yield of PSII obtained by PAM fluorometry.
F_v/F_{mFRRf}: Maximum quantum yield of PSII obtained by FRR fluorometry.

Appendix A

Station	θ between σ_θ = 26.7-26.8
Bio-1	0.6
Bio-2	0.6
Bio-4	3.5
Bio-6	2.3
Bio-7	1.1
Bio-9	1.3
Bio-10	1.0
Bio-11	0.9
Bio-12	1.3
Bio-13	4.0
Bio-14	0.5
AK15-1	ND
AK15-2	ND

Appendix B

Station	Chl c_3	Chl c_2	Chlide *a*	Peri	19'-BF	Fuco	Neo	Prasino	Viola	19'-HF	DD	Allo	DT	Zea	Lut	Chl *b*	Chl *a*	α, β-caro
Bio-1	0.0324	0.0467	0.0240	0.0248	0.0286	0.138	0.0060	0.0114	0.0104	0.0210	0.0536	0.0015	0.0037	0.0041	0.0016	0.0393	0.286	0.0144
Bio-2	0.0321	0.0522	0.0213	0.0327	0.0337	0.113	0.0061	0.0094	0.0104	0.0314	0.0473	UD	0.0034	0.0042	0.0010	0.0365	0.248	0.0169
Bio-4	0.0336	0.0907	0.0411	0.0725	0.0208	0.281	0.0103	0.0155	0.0131	0.0163	0.0755	UD	0.0059	0.0090	0.0026	0.0600	0.371	0.0310
Bio-6	0.0231	0.0900	0.0428	0.113	0.0156	0.232	0.0086	0.0112	0.0124	0.0093	0.0820	UD	0.0104	0.0091	0.0016	0.0470	0.639	0.0321
Bio-7	0.0199	0.0555	0.0185	0.0522	0.0132	0.160	0.0056	0.0098	0.0089	0.0086	0.0593	UD	0.0094	0.0047	0.0016	0.0459	0.280	0.0240
Bio-9	0.0323	0.0951	0.0500	0.0687	0.0238	0.277	0.0099	0.0175	0.0186	0.0167	0.0822	0.0018	0.0071	0.0076	0.0032	0.0667	0.438	0.0285
Bio-10	0.0257	0.0354	0.0251	0.0202	0.0254	0.0839	0.0038	0.0087	0.0038	0.0300	0.0379	UD	0.0116	0.0072	0.0023	0.0306	0.256	0.0112
Bio-11	0.0360	0.0828	0.0380	0.0371	0.0344	0.219	0.0077	0.0128	0.0157	0.0386	0.0624	0.0006	0.0052	0.0061	0.0031	0.0559	0.386	0.0273
Bio-12	0.0408	0.0985	0.0499	0.0706	0.0388	0.265	0.0095	0.0182	0.0216	0.0288	0.0902	0.0016	0.0089	0.0087	0.0032	0.0753	0.404	0.0314
Bio-13	0.0743	0.1506	0.0686	0.0964	0.0841	0.282	0.0104	0.0169	0.0238	0.0784	0.127	UD	0.0098	0.0077	0.0058	0.0761	0.647	0.0421
Bio-14	0.0537	0.2949	0.1635	0.0556	0.0389	1.13	0.0148	0.0202	0.0210	0.0249	0.162	0.0018	0.0153	0.0097	0.0043	0.100	1.28	0.0679
AK15-1	0.0233	0.0064	UD	0.0469	UD	2.11	0.0060	UD	UD	0.0106	0.219	0.110	0.0108	0.0083	UD	0.0631	4.76	0.0794
AK15-2	0.0195	0.0068	UD	0.0880	UD	3.08	0.0101	UD	UD	UD	0.218	0.0661	0.0222	UD	UD	0.0634	6.22	0.0920
Bio-6_Ini	0.0231	0.0900	0.0428	0.113	0.0156	0.232	0.0086	0.0112	0.0124	0.0093	0.0820	UD	0.0104	0.0091	0.0016	0.0470	0.639	0.0321
Bio-6_Con	0.0113	0.0113	UD	0.143	0.0139	0.245	UD	0.0124	UD	0.0132	0.0627	0.0506	UD	UD	UD	0.0361	0.801	0.0194
Bio-6_+7ºC	UD	UD	UD	0.164	0.0130	0.201	0.0042	0.0111	UD	0.0123	0.0534	0.0481	UD	UD	UD	0.0308	0.740	0.0180
Bio-7_Ini	0.0199	0.0555	0.0185	0.0522	0.0132	0.160	0.0056	0.0098	0.0089	0.0086	0.0593	UD	0.0094	0.0047	0.0016	0.0459	0.280	0.0240
Bio-7_Con	0.0103	0.0146	UD	0.0170	0.0053	0.0867	0.0024	0.0047	UD	0.0047	0.0138	0.0101	UD	UD	UD	0.0136	0.222	0.0054
Bio-7_+7ºC	UD	UD	UD	0.0219	0.0056	0.0870	0.0029	0.0050	UD	0.0049	0.0133	0.0094	UD	UD	UD	0.0152	0.229	0.0053
Bio-10_Ini	0.0257	0.0354	0.0251	0.0202	0.0254	0.0839	0.0038	0.0087	0.0038	0.0300	0.0379	UD	0.0116	0.0072	0.0023	0.0306	0.256	0.0112
Bio-10_Con	UD	UD	UD	0.0267	0.0274	0.0933	0.0033	0.0048	0.0055	0.0300	0.0289	0.0124	UD	UD	UD	0.0272	0.353	0.0073
Bio-10_+7ºC	0.0210	0.0227	UD	0.0189	0.0214	0.0761	UD	0.0075	UD	0.0225	0.0157	0.0076	UD	UD	UD	0.0369	0.324	0.0101
Bio-13_Ini	0.0743	0.151	0.0686	0.0964	0.0841	0.2818	0.0104	0.0169	0.0238	0.0784	0.127	UD	0.0098	0.0077	0.0058	0.0761	0.647	0.0421
Bio-13_Con	0.0930	0.0827	UD	0.111	0.0695	0.2465	0.0068	0.0164	0.0148	0.0632	0.0658	0.0598	UD	UD	UD	0.0544	0.857	0.0241
Bio-13_+7ºC	UD	0.0440	UD	0.112	0.0638	0.2145	0.0062	0.0147	0.0127	0.0569	0.0538	0.0541	UD	UD	UD	0.0524	0.774	0.0197

Appendix C

Station	$F_v/F_{m\ FRRf}$	σ_{PSII}	[RCII]
	–	× nm^2 $PSII^{-1}$	× 10^{-9} mol m^{-3}
Bio-1	0.582	2.69	0.49
Bio-2	0.322 ± 0.064	3.78 ± 0.64	1.54 ± 0.84
Bio-4	0.421 ± 0.024	2.79 ± 0.16	1.04 ± 0.20
Bio-6	0.467 ± 0.068	2.56 ± 0.19	1.50 ± 0.31
Bio-7	0.515 ± 0.064	2.85 ± 0.15	0.76 ± 0.33
Bio-9	0.394 ± 0.026	2.91 ± 0.16	1.23 ± 0.25
Bio-10	0.377 ± 0.050	3.06 ± 0.30	0.62 ± 0.11
Bio-11	0.504 ± 0.033	2.78 ± 0.14	1.24 ± 0.12
Bio-12	0.475 ± 0.049	3.01 ± 0.08	1.15 ± 0.27
Bio-13	0.432 ± 0.020	3.13 ± 0.19	1.94 ± 0.16
Bio-14	0.477 ± 0.005	2.43 ± 0.15	5.57 ± 0.22
AK15-1	ND	ND	ND
AK15-2	ND	ND	ND

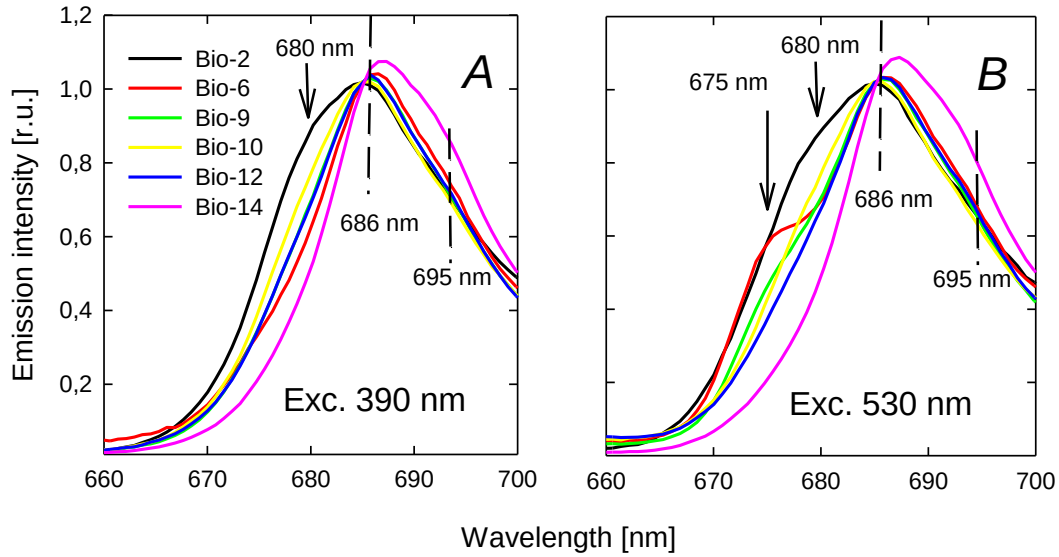
A
B
Bio-2
Bio-6
Bio-9
Bio-10
Bio-12
Bio-14
680 nm
675 nm
686 nm
695 nm
Exc. 390 nm
Exc. 530 nm
Emission intensity [r.u.]
Wavelength [nm]

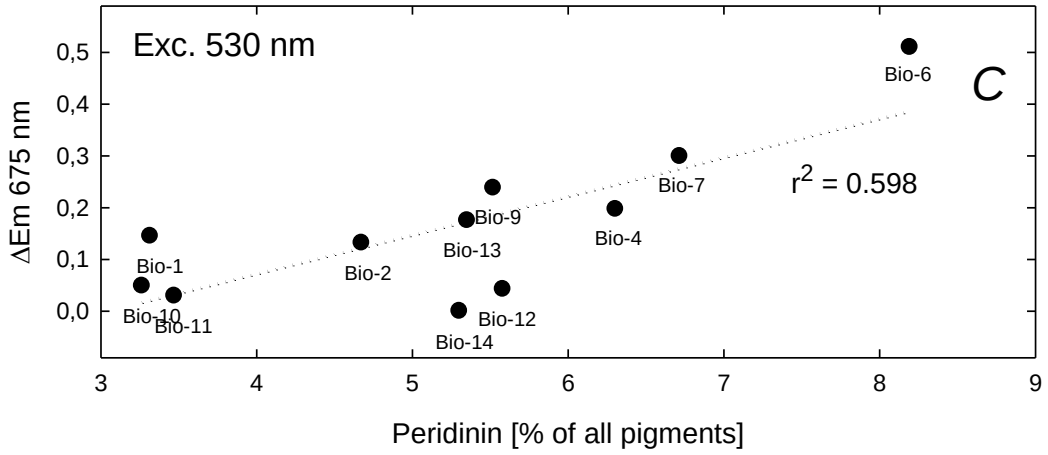
Exc. 530 nm
C
Bio-6
Bio-7
Bio-9
Bio-4
Bio-13
Bio-1
Bio-2
Bio-10
Bio-11
Bio-12
Bio-14
r2 = 0.598
ΔEm 675 nm
Peridinin [% of all pigments]

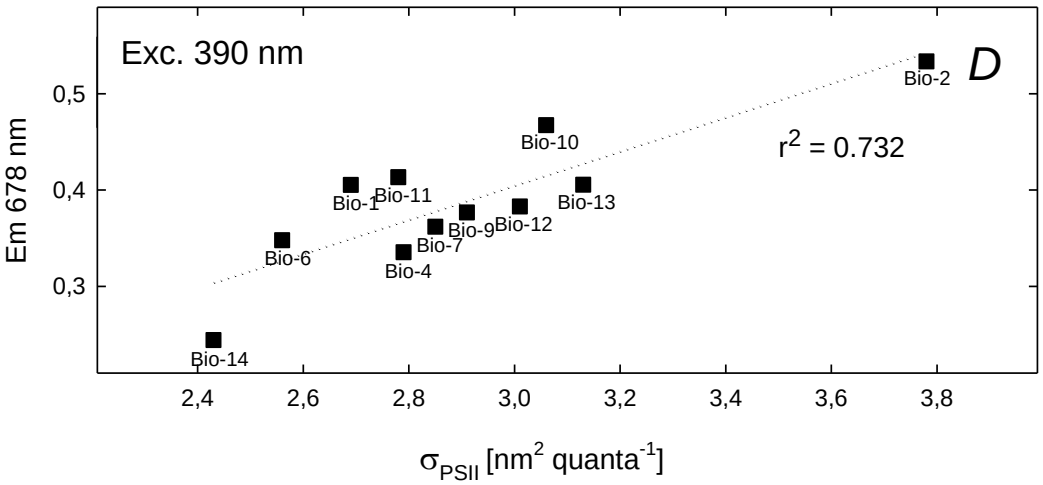
Exc. 390 nm
D
Bio-2
Bio-10
Bio-1
Bio-11
Bio-13
Bio-9
Bio-12
Bio-6
Bio-7
Bio-4
Bio-14
r2 = 0.732
Em 678 nm
σPSII [nm2 quanta-1]

Appendix D

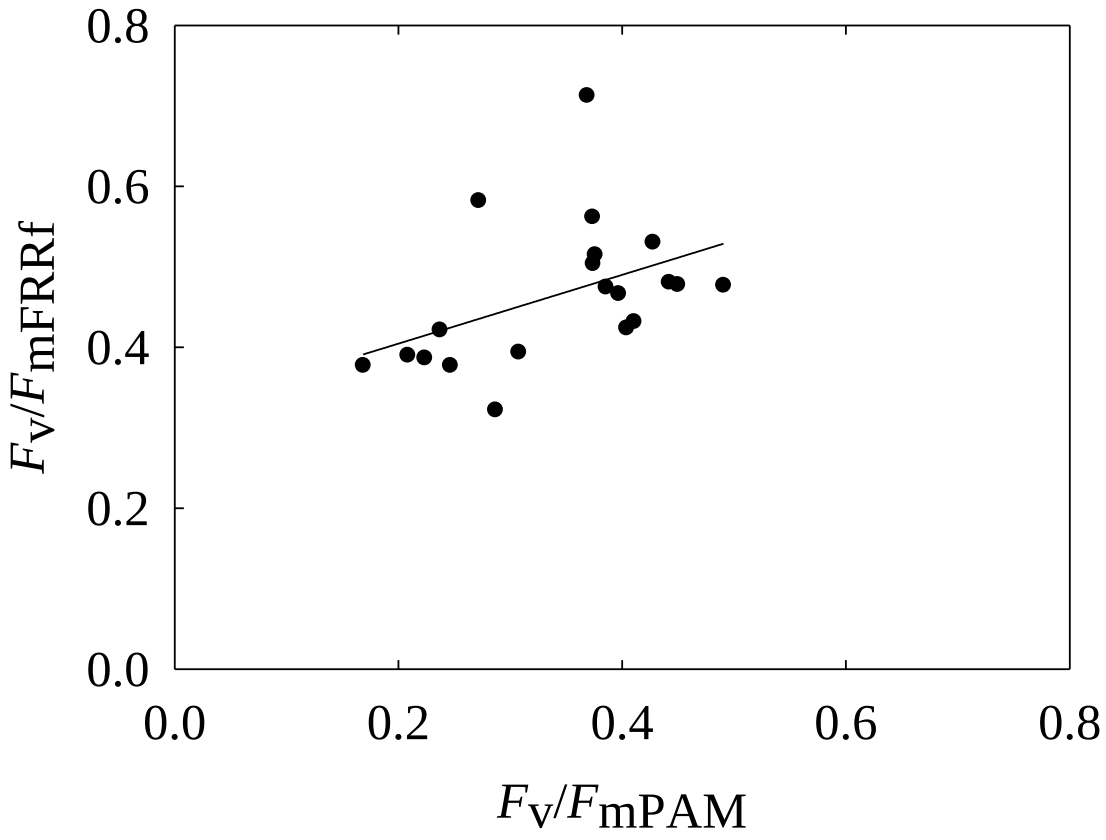

Appendix E.